Devitrification Kinetics and Optical Stability of Optical Fibers at High Temperatures

Anastasia A. Yakusheva

Thesis submitted to the faculty of the Virginia Polytechnic Institute and State University in partial fulfillment of the requirements for the degree of

Master of Science

In

Materials Science and Engineering

Gary Pickrell, Chair

Daniel Homa

Anbo Wang

May 2, 2018

Blacksburg, VA

Keywords: fused silica, fiber optics, harsh environments, devitrification

Copyright © 2018 Anastasia Yakusheva

Devitrification Kinetics and Optical Stability of Optical Fibers at High Temperatures

Anastasia A. Yakusheva

ABSTRACT

Reliable sensing and monitoring systems based on optical fibers operating at high temperatures and in harsh environments are of high demand. One of the limitations of such systems is the devitrification of the fused silica based core and cladding glass at elevated temperatures. Crystallites can nucleate on the surface of the cladding and grow into the core. The formation of these crystalline flaws in the optical fiber causes stress concentration and extrinsic optical scattering and in addition leads to decreased mechanical properties and reduced optical stability. Commercial optical fibers of different compositions and core-cladding design were characterized in this study with respect to crystallization rate under various conditions. The optical stability was monitored with an optical spectrum analyzer. The crystallites were characterized with SEM and optical microscopy. The activation energies of crystallization for High OH and Low OH multimode fibers were estimated by measuring the crystal growth rate at different temperatures. The residual stress resulting from the formation of the crystals, which can lead to decreased mechanical performance of the fibers, was characterized with polarized light optical microscopy. The influence of water vapor in the atmosphere on the crystallization rate was determined. The features induced in the attenuation spectra were consistent with hydroxyl (OH) absorption peak. Spectral features such as thermal emission and hydroxyl absorption bands are discussed.

The results obtained in this study can be used for selecting optical fibers for high temperature applications.

Devitrification Kinetics and Optical Stability of Optical Fibers at High Temperatures

Anastasia A. Yakusheva

GENERAL AUDIENCE ABSTRACT

Reliable sensing and monitoring systems based on glass optical fibers operating at high temperatures and in harsh environments are in high demand. One of the limitations of such systems is the tendency of glass material to crystallize at elevated temperatures.

Crystallites can nucleate on the surface of the fiber and grow inwards, impairing the optical and mechanical properties of the optical fiber. The formation of these crystalline flaws in the optical fiber can decrease the mechanical strength by causing stress concentrations and leading to formation of cracks, and reduce optical stability by causing light to scatter from the crystals. Commercial optical fibers of different compositions and geometry were characterized in this study with respect to crystal growth rate under various conditions, such as different temperatures (400-1350 °C), and different atmospheres (laboratory air and water vapor). The effect of crystals was demonstrated with respect to optical and mechanical performance.

The results obtained in this study can be used for selecting optical fibers for high temperature applications.

CONTENTS

INTRODUCTION

Motivation

Energy consumption is steadily rising and there is considerable interest to move to the development of cleaner technologies, and improve, diversify, and increase the efficiency of domestic energy production in order to reduce carbon pollution and greenhouse gas emission. [1]

Energy conversion systems such as solid oxide fuel cells, combustion turbines and advanced boiler systems are becoming increasingly complex and are subject to harsher environments (shown in Table 1), as energy efficiency is improved and emissions and safety regulations are implemented. Therefore, advanced sensor and monitoring systems operating at high temperatures are a necessary component to meet the performance standards and safety regulations. [2]

Table 1. Power Generation Technology Needs [2]

	Coal Gasifiers	Combustion Turbines	Solid Oxide Fuel Cells	Advanced Boiler Systems
Temperature	< 1600 C	< 1300 C	< 900 C	< 1000 C
Pressures	< 1000 psi	Ratios 30:1	Atmospheric	Atmospheric
Atmosphere(s)	Highly Reducing Erosive, Corrosive	Oxidizing	Oxidizing and Reducing	Oxidizing
Examples of Important Gas Species	H_2, O_2, CO, CO_2, H_2O, H_2S, CH_4	O_2, Gaseous Fuels (Natural Gas to High Hydrogen), CO, CO_2, NO_x, SO_x	Hydrogen from Gaseous Fuels and Oxygen from Air	Steam, CO, CO_2, NO_x, SO_x

Along with high temperatures, the presence of humidity in these energy conversion systems presents challenges for durable sensing devices: for example, the presence of hydrogen and

humidity in solid oxide fuel cells in the reformed gases presents a challenge to monitoring the gaseous species that are damaging to the systems components. [3]

The advancements in nuclear power plants are a way to reduce CO_2 emissions [1], as the process generates no CO_2 emissions and so none are released into air. However, several technical challenges limit these advancements. For example, advanced small modular reactors operate at much higher temperatures than conventional lightwater reactors, and therefore, require the instrumentation capable of withstanding harsh environments. The technical concepts of water reactors monitoring systems are out-of-date and are not applicable to advanced reactor designs, and therefore needed to be reevaluated. [1]

Conventional electronic sensing systems do not satisfy the harsh environment design demands, as they require conductive pathways, can be subject to electromagnetic interference, and require additional packaging at the temperatures in excess of 400°C, which in turn leads to increased cost of operation. The breakthrough in optical-based sensing technologies have the potential to meet these demands, as the new optical materials and purification methods are developed. [4] Fiber optic sensors are lightweight, compact, immune to electromagnetic fields interference, and do not require electrically conductive pathways.

A variety of fiber optic sensors has been developed, including Fabry-Perot interferometers, fiber Bragg gratings, as well as distributed sensing systems based on Rayleigh and Raman backscatter.

Fabry-Perot interferometer based fiber optic sensors are typically used for temperature, strain and pressure sensing. [5] They operate by measuring the shift in optical interference fringes, that depends on the Fabry-Perot cavity length, which in turn is affected by temperature and pressure

changes. The upper temperature limit for Fabry-Perot sensors were demonstrated to be up to 1000° C. [4]

Fiber Bragg grating sensors are widely used for distributed temperature and strain monitoring. [6] The grating is the alteration of the refractive index in the core with a specific period, that defines the reflected wavelength (Bragg wavelength). The grating period as well as the effective refractive index is affected by the sensing parameters (strain or temperature); and this causes the Bragg wavelength to shift, which allows measurement of the change in temperature or strain.

Distributed sensing based on the Rayleigh scattering effect uses the reflections of the laser pulse from the unique pattern of density fluctuations in the fiber. The OTDR (optical time-domain reflectometry) technique that utilizes the backscatter signals of a laser pulse as a function of time delay, that defines the locations of these events. Strain or temperature stretches the pattern of the fiber, which results in the shift of the backscatter signal, and by measuring this shift it is possible to perform sensing. The OFDR (optical frequency-domain reflectometry) is the interferometric technique that uses a tunable laser source and measures the reflection events as a function of frequency, that is then Fourier-transformed to obtain the time-of-flight values, and consequently the locations of these events. The most widely used technique for distributed temperature sensing is Raman backscattering reflectometry. It measures inelastic scattering events of the laser pulse from the vibrations and compares the anti-Stokes component, that is temperature-sensitive, to the reference Stokes component (temperature insensitive). [4]

Fused silica optical fibers are widely used for sensing applications. Single mode fibers are generally used for distributed and semi-distributed sensing. They give very high sensitivity, as

having a single mode allows them to construct guided wave interferometers directly from the fiber itself so as to measure small phase changes in light transmitted through the measuring region. [42] Multi mode optical fibers are generally used in intensity-based sensors, as they allow more power to be confined. [47] Commercially available sapphire optical fibers are also multimode in nature, and suitable for harsh environment applications (discussed in the following chapter). [46]

Current State and Limitations

Single crystal sapphire fibers possess unmatched corrosion resistance and long-term stability for high temperature sensing (in excess of 1500 °C), but the cost and expertise required for their use has cultivated renewed interest in alternative solutions that rely on lower cost fused silica based optical fibers. [7]

The main limitation for the use of fused silica fibers at temperatures in the range 400 ºC – 1000 ºC and above is related to decreased optical and mechanical performance. Although the optical fiber coating often precludes their use at temperatures in excess of 400 ºC, an increasing number of niche applications have been explored for the use of fused silica based optical fibers at temperatures approaching 1100 ºC. [8-10]

The interaction of fused silica glass with chemical constituents of the environment of sensor deployment induces the absorption windows at specific wavelengths throughout the spectrum and therefore reduces optical stability. Certain pollutant gases such as nitric oxide (NO) and nitrogen dioxide (NO_2) have fundamental absorption lines in the mid-infrared region, and carbon containing gases (CO and CO_2) also have fundamental absorptions in the infrared. Moreover, these species can incorporate and react with the glass network. Oxygen molecules, for example, are known to react with oxygen vacancies in silica glass to form peroxy linkages. [12] The most studied case is the hydrogen (or the hydroxyls which may form) absorption band in the near infrared, which is crucial for telecommunication and sensing applications. Telecommunications wavelength windows are shown in Table 2.

Table 2 Wavelength regions used in optical fiber communications: "Telecom windows"

Band	Description	Wavelength Range
O band	Original	1260 – 1360 nm
E band	Extended	1360 – 1460 nm
S band	Short wavelengths	1460 – 1530 nm
C band	Conventional ("erbium window")	1530 – 1565 nm
L band	Long wavelengths	1565 – 1625 nm
U band	Ultralong wavelengths	1625 – 1675 nm

Incorporation of molecular water (H_2O) and hydroxyl (OH) will weaken the glass network and increase the attenuation of optical fibers at specific wavelengths. Formation of Si-OH at defect sites is vibrational in nature and its fundamental overtones, centered at 1.385 μm, cause absorption peaks throughout the entire optical transmission spectrum of fused silica, the infrared absorption spectra summarized in Table 3 [13].

Table 3 OH, H_2O and their combination vibrations in fused silica glass [13]

Assignment	Wave number (cm^{-1})	Wavelength (nm)	Description
υ_1(OH) +υ_4(SiO4)	4100	2439	Combination of fundamental OH stretching and fundamental SiO4 vibrations

υ_1(OH) +υ_4(SiO4)/ $\upsilon_{comb,2}(OH)$	4450	2247	Combination of fundamental OH stretching and fundamental SiO4 vibrations/asymmetric distribution of silanol vibration due to hydrogen-bond
υ_4(OH) +υ_3(SiO4)/ $\upsilon_S(SiOH)$ + $\upsilon_B(SiOH)$	4520	2212	Combination of fundamental OH stretching and fundamental SiO4 vibrations/combination fundamental OH stretching and SiOH bending
$\upsilon_B(H2O)_l$ +$\upsilon_{SS}(H2O)_l$	5102	1960	Possibly, combination of bending and symmetric stretching band of Type I molecular water
$\upsilon_S(H2O)_l$ +$\upsilon_{AS}(H2O)_l$	5249	1905	Combination of bending and stretching of molecular water, or more specifically, bending and asymmetric stretching of Type I molecular water
$\upsilon_S(GeOH)$	7042	1420	OH stretching vibration bonded to Ge site
$2\upsilon_3(OH)$	7100	1408	First overtone OH stretching
$2\upsilon_2(OH)$	7220	1385	First overtone OH stretching
$2\upsilon_1(OH)$	7260	1377	First overtone of OH stretching
$2\upsilon_3(OH)$ + υ_2(SiO$_4$)	7380	1355	Combination first overtone OH stretching and fundamental SiO4 vibration
$2\upsilon_3(OH)$+ $\upsilon_1(SiO_4)$	7920	1263	Combination first overtone OH stretching and fundamental SiO4 vibration
$2\upsilon_1(OH)$ + $\upsilon_1(SiO_4)$	8065, 8130	1230, 1240	Combination first overtone OH stretching and fundamental SiO4 vibration
$2\upsilon(OH)$ + 2υ $(SiO4)$	8889	1125	Combination first overtone OH stretching and first overtone SiO4 vibration

Another reason for decreased optical stability at elevated temperatures is the mobility of dopant atoms (generally F, Ge, P). The diffusion of germanium or phosphorus towards the cladding, or fluorine or boron inwards towards the core, changes the radial distribution and broadens the core, affecting the waveguide properties. Expanding of the core changes the modal-

field distribution along the fiber. [14] The number of supported modes in the fiber is defined by the *V*-number, that is proportional to the numerical aperture *NA*, that in turn is defined by the difference between the indices of refraction of the core and cladding:

$$V = \frac{2\pi}{\lambda} a\, NA = \frac{2\pi}{\lambda} a \sqrt{n_{core}^2 - n_{cladding}^2} \quad (1)$$

For multimode fibers, that have a V-number much higher than 2.405, the number of supported modes is approximated as:

$$M \approx V^2/2 \quad (2)$$

Therefore, as the dopants diffuse inwards or outwards, the difference between the indexes of refraction of cladding and core decreases, and therefore the number of supported modes decreases, making a fiber sensitive to micro-bend losses and to absorption losses in the cladding. [39]

The tendency of fused silica glass fibers to crystallize at temperatures approaching the glass transition temperature is another main limitation in use of silica based optical fibers at elevated temperatures. This phenomenon is known to occur in silica glass and has been studied for bulk samples, but there is limited knowledge in this area for optical fibers [8-10]. Crystalline SiO_2, in the form of cristobalite, typically nucleates heterogeneously at defect sites (cracks, contamination, H_2O, impurities) on the surface of the fiber and propagates along the surface and inward towards the fiber core causing a broadband scattering loss that continues to increase with

the progression of crystallization [8-10]. Depolarization from scattering could be another consideration for optimum sensitivity. [9] Moreover, induced thermal mismatch between amorphous fused silica glass and crystallized regions can lead to stress-induced loss, and the presence of crystallized inclusions can possibly cause microbending losses. [9] Furthermore, thermal mismatch between the glass and crystals results in degradation of mechanical properties of the optical fiber: it induces micro crack formation upon changes in temperature. Another reason for the reduction of mechanical strength of the fused silica optical fibers is that the cristobalite crystals on the surface of the fiber act as stress concentrating flaws. [22]

The potential impact of induced crystallization and optical losses must be thoroughly evaluated and understood to be able to reliably predict the performance at these temperatures for the sensing systems.

Literature review

Crystallization in bulk silica glass has been experimentally investigated and reported by many researchers.

Wagstaff et al. [16] performed a comprehensive study of intrinsic crystallization kinetics in stoichiometric silica glass. It was experimentally shown that the crystallization is controlled by three reactions. First, intrinsic crystallization was investigated in vacuum furnace, with minimized amount of impurities. The intrinsic crystallization rates were shown to be the lowest. Intrinsic crystallization was also investigated in dry nitrogen atmosphere, and shown that it heavily depends on the contamination content, that could be controlled in those experiments. The second reaction occurs from sites with adsorbed impurities, and this increases the crystallization rate more significantly the higher the temperature. Finally, the third control mechanism is the effect of water vapor. The data was analyzed at high partial pressure of water, so the unknown variables of intrinsic and contamination impurities contributions can be neglected. The glass used in the experiments was Type III vitreous silica, which is not typically used in optical fibers.

Optical fiber devitrification during fusion splicing has been studied by Tachikura et al [30]. It was shown that diffusion-controlled kinetics was the growth mechanism for both cases with and without contamination: crystallite growth was either controlled by the diffusion of contaminations in the glass introduced in the experiment, or by the diffusion of impurities present in the glass internally (crystalline diameter is proportional to square root of heating time). It was concluded that consequent tensile strength reduction is proportional to the fourth root of heat treatment time. It was shown, that the heating temperature crucially affects the devitrification of the optical fibers, as well as electrode gap affects the position of the break

during tensile test.

Rose et al. [10] showed that the presence of OH in the glass contributes to crack formation and devitrification through decreasing the glass viscosity. They also performed spectral measurements showing the OH absorption peak appearing at 950 °C, however, no kinetic dependences were studied.

The correlation of crystal formation on the fiber surfaces with the decrease in mechanical properties has been reported. Study by Lezzi et al. [22] The study includes commercially available silica glass fibers as well as manually drawn glass fibers of different silica types. It was shown that crystallization occurs at temperatures as low as 500 °C and crystallization kinetics were evaluated with a scanning electron microscope (SEM). The strength degradation kinetics were also studied and shown to be induced by surface crystallization at temperatures in excess of 800 °C, through thermal stresses formed during cooling, due to thermal expansion mismatch. The crystal growth rates (along with fracture strengths) as functions of time were found to be linear, in agreement with previous studies in bulk.

The study by Zheng [31] also shows that defects on the fiber surface significantly affect the fiber tensile strength. It concludes that the mechanical performance decrease occurs in two stages. First, at lower temperatures, around 600 °C, the tensile strength of the fibers reduces due to the fact that the polymer coating is completely burned off and the inherent defects are exposed on the surface. Second, at temperatures of 700 – 900 °C, the formation of "strip" defects and nanometer-scale ordered regions are observed with the transmission electron microscopy (TEM) study. X-Ray diffraction data shows the peak at the α-cristobalite location. The study does not include any quantitative kinetic data.

Since it has been extensively reported that the introduction of OH into the silica glass promotes devitrification through reduction of glass viscosity [10] and breaking the silicon-oxygen bonds, it is necessary, along with investigating the crystal growth and formation, to study the OH-related effects in the optical spectrum. The cases of interaction of chemical constituents with the fused silica of the optical fibers and induced absorption peaks were described in the previous chapter, including the hydrogen absorption band in near infrared.

Rose et al [9] showed the decreased optical performance of fused silica (the fiber cladding is SiO_2 and the single mode core is about 4 mole % doped GeO2:SiO2 glass) optical fibers is attributed to devitrification of the surface, and OH absorption at elevated temperatures in the infrared region was demonstrated. It was experimentally shown, that transmittance of optical fibers rapidly decreases at the temperatures exceeding 1000 °C. It is also shown that significant crystallization takes place at temperatures above 850 °C. With the new the advancements of optical fiber drawing technology, these results need to be reevaluated for the optical fibers currently present in the market. The transmittance characterization does not show any spectral information that could be crucial for high-temperature applications.

It was also described in the literature [28] that when the temperature approaches 1000 °C optical fiber spectrum shows peaks at 1260 and 1390 nm attributed to thermal luminescence of hydroxyl in the fiber, with the peak at 1390 being temperature-dependent up to 1000 °C (for pure silica core, moderately fluorine-doped and extensively fluorine-doped silica core and fluorine-doped silica cladding) . It was shown that the intensity of the peak changes with time as the fiber is held at 1000 °C, which is attributed to thermal radiation of the furnace through the cladding of the fiber damaged by the nucleation and growth of the crystals. However, when the temperature

was decreased to 900 °C, no thermal radiation except for OH luminescence was generated and the spectral shape remained unchanged.

Yokomachi et al [29] also described optical spectral changes around 1.39 nm, the first overtone of OH-stretching vibration. It was demonstrated that the absorption caused by the OH group stretching increases with increasing temperature. But during the second cycle of heat treatment it was observed that the absorption peak changes its shape, having a component with the “negative” induced loss.

Therefore, response in the optical spectrum in the near infrared to the elevated temperatures should be evaluated, along with the kinetics of crystallization.

EXPERIMENTAL PROCEDURE

In order to investigate devitrification behavior in optical fibers, several commercial fused silica fibers of different geometries and composition were heat treated in ambient air and water vapor atmospheres. Their optical performance along with surface effects was monitored as a function of time and temperature.

The samples to be tested (as shown in Table 4) are step index fused silica optical fibers. FG105UCA, FG105LCA and FG105ACA are multimode fibers with pure silica core and fluorine doped silica cladding with different OH content, purchased from Thorlabs. Their applications include spectroscopy for pollution analysis and chemical processing, medical diagnostics, and power delivery applications. The standard single mode fiber (SMF) was manufactured by Spectran, and maintains a germanium-doped silica core and pure silica cladding fiber, it's typical applications include sensing, instrumentation, and telecommunication.

Table 4. Commercial Optical Fibers Tested

Fiber ID	d_{core} (μm)	d_{clad} (μm)	NA	Relative [OH]
FG105UCA	105	125	0.22	High
FG105LCA	105	125	0.22	Low
FG105ACA	105	125	0.22	High
Spectran SMF	8.3	125	0.14	Low

Fibers were heated to a range of temperatures of 400 °C – 1200 °C, in MTI GSL-1100X and 1800 °C-Deltech tube furnaces, for different durations. For the first set of experiments annealing was conducted in laboratory air, and then the bubbler setup was added to provide exposure to water vapor (the estimated volume flow of approximately 0.22 ml/min, bubbler temperature of

approximately 100 °C), as shown schematically in Figure 1. The bubbler was added in order to experimentally investigate the effects of water vapor on the performance of optical fibers: surface characterization along with optical transmittance spectra were collected, as the previous studies have shown that water vapor can enhance crystallization in bulk silica glass.

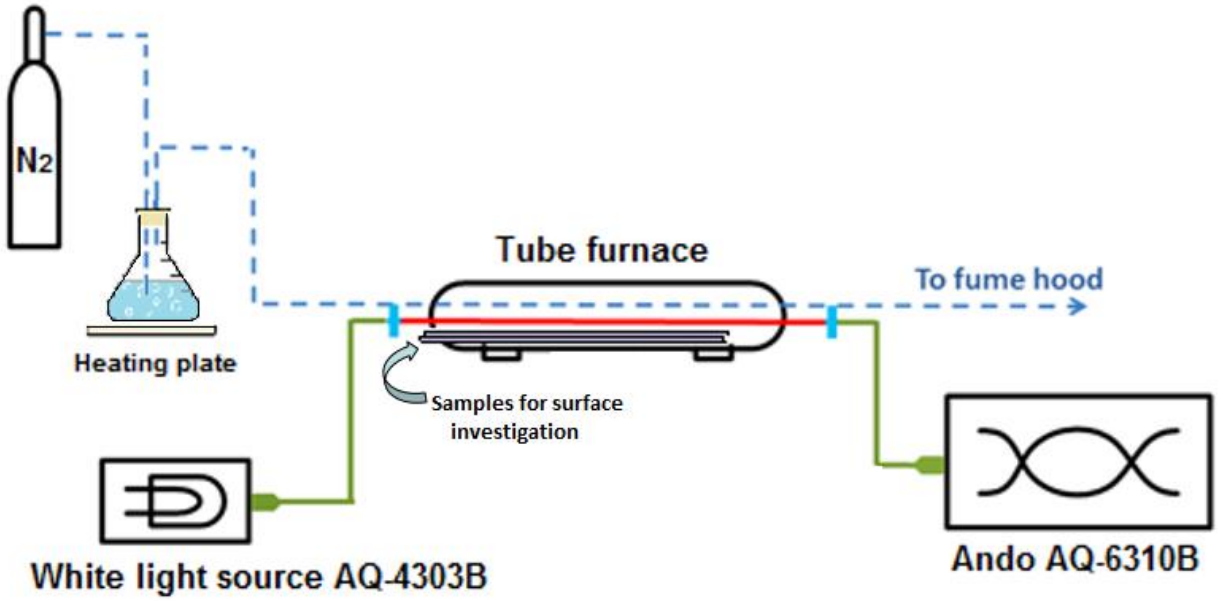

Figure 1. Schematic diagram of the system where fibers were heat treated with and without exposure to nitrogen humidified with water vapor

The acrylate coating over the cladding layer was removed by soaking the fibers in acetone prior to the heat treatments, as the operating temperature of the fibers (coating) is much lower that the temperatures reached for these experiments (85 °C for acrylate and 150 °C for high temperature acrylate). As the coating carbonizes and flakes off below 400 °C, it has no effect on the experiments above this temperature, including stress-induced loss or microbending effects, that were shown to be reversible [9], Moreover, the removal of the coating prevents the furnace from being contaminated. The length of the heating region of the furnace is approximately 15 cm, and the samples for surface investigation were cut out from this length.

Optical spectra were collected in-situ using an Ando AQ-6310B optical spectrum analyzer and AQ-4303B white light source; spectra wavelengths ranged from 400 nm to 1800 nm. The optical spectrum of the "as received" fibers was selected as the baseline for all the analyses. Furthermore, the calculated loss (dB) neglects any loss due to the low temperature regions on both ends of the furnace's 15 cm heating length.

For each test, sample fibers were removed from the furnace at specified time intervals in order to observe the kinetics of surface effects. It improved the efficiency (as the furnace was operated only once to obtain the set of samples), as well as the reliability of the experiment, as all the fibers, including the one for in-situ monitoring of optical performance, were heat-treated in the same conditions.

The images of the fiber surfaces were obtained with an FEI Quanta 600 FEG environmental SEM, which allows imaging the surface features with submicron resolution as well as imaging a large area. Later in the experiment for the specimens with confirmed surface morphology effects of a large scale, an optical microscope Olympus BX51 was used.

ImageJ software was employed for the analysis of microscopy data. Determination of the diameter of the crystallites and calculation of the percent of crystallized fiber surface was performed.

HEAT TREATMENT IN AIR

The first set of experiments was performed in ambient air with several pure silica core multimode fibers. The induced loss, shown below, is defined as the difference between the recorded spectra and the baseline measurement at room temperature, so that the Induced loss (dB) neglects any loss due to the low temperature regions on both ends of the furnace's 15 cm heating length.

Preliminary Tests

Solarization resistant fiber FG105ACA was exposed to the temperatures of 400 ºC and 1000 ºC for the initial monitoring of optical performance. It was observed, that there is no broadband loss induced over the duration of the tests (36 hours and 73 hours respectively), as shown in Figure 2.

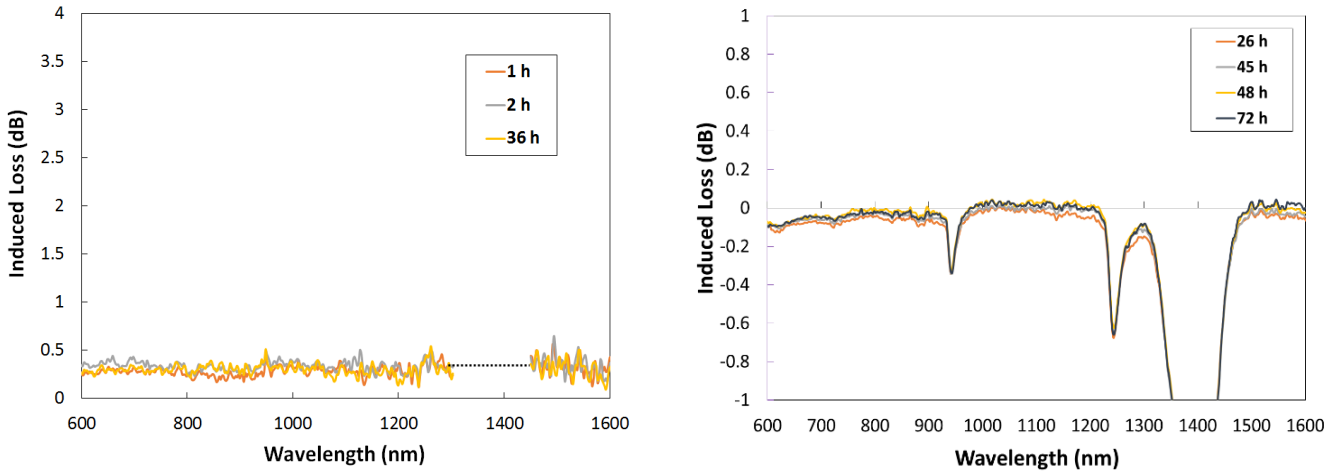

Figure 2. Induced loss spectra of FG105ACA at a) 400° C and b) 1000° C. ***Please note that the limited dynamic range of the optical spectrum analyzer did not allow for the accurate measurement of the OH overtone centered at ~1390 nm for optical fibers with a relative high OH content.***

However, several features in the optical spectra due to high temperature exposure were observed. A “negative” induced loss was observed at hydroxyl absorption peak positions at 1000 ºC, and are attributed to a thermal emission process [12, 13]. The emission peak positions (Fig. 2 (b)) are consistent with the first, second, and third hydroxyl overtones (985 nm, 1240 nm, and 1390 nm, respectively) of the fundamental Si-OH absorption at ~2850 nm [11].

Even though from optical transmittance data it can be concluded that there were no crystallites grown large enough to reach the core (the experimental data of the heat treated fiber cross section is presented in the following chapter), and therefore cause broadband scattering loss, as well as there was no evidence in the optical spectrum of the crystals induced stress that reached the core, it is still important to investigate the surface, as even the formation of small crystallites can lead to decreased mechanical performance. The crystallites on the surface of the fiber were found even at the temperature as low as 400 °C (as shown in Figure 3 (a)). For comparison, SEM microimage of the same decoated fiber before the heat treatment is shown in Figure 3 (b). The fiber was investigated throughout the length of the sample and no irregularities of the surface were found, except for impurity particles attached the surface (white dots), that can also be observed at higher temperatures. The crystal growth rate (Figure 3 (b)) was obtained by measuring the crystal diameter (length) along the longer axis, and as expected the rate was higher at the higher temperature, as shown in Figure 3 (c), which is consistent with the literature [8, 10]. The crystals of cristobalite were observed to nucleate and grow, having nonuniform shape with the bumps, but without the formation of cracks.

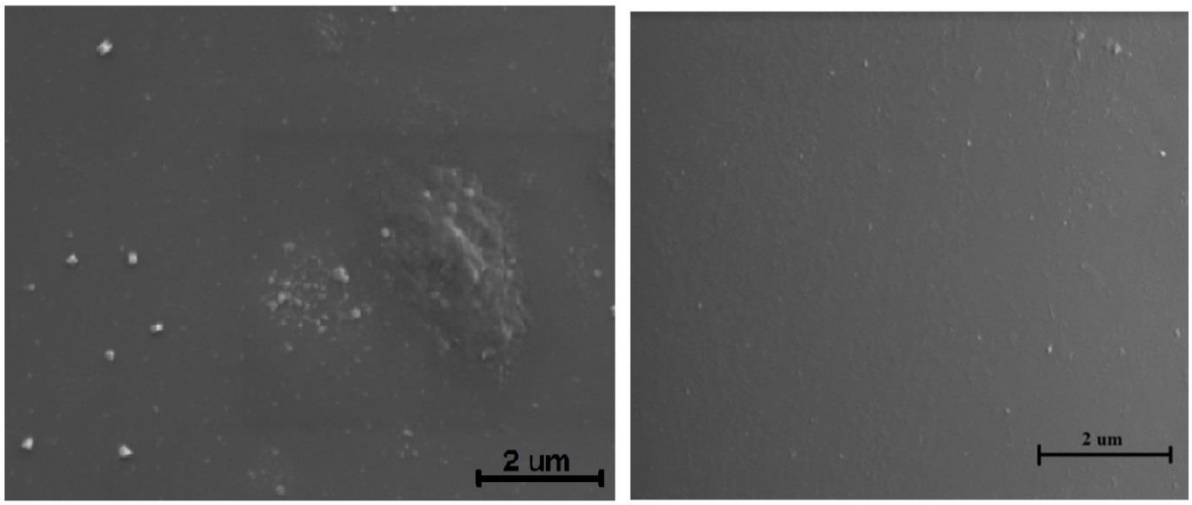

(a) **(b)**

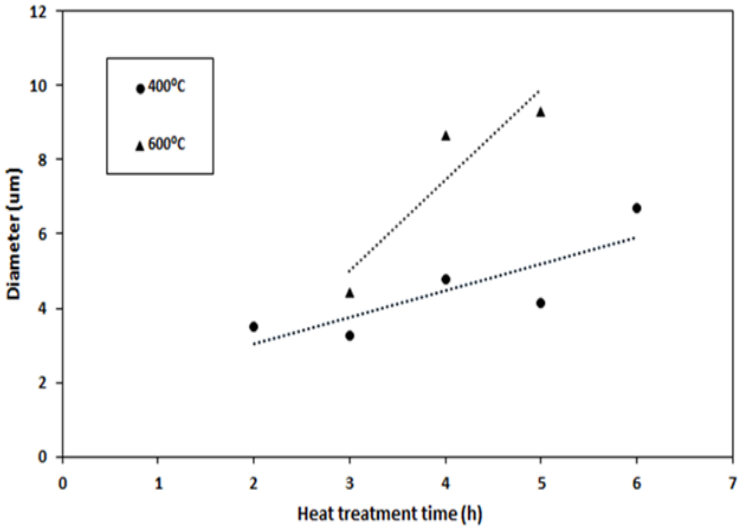

(c)

Figure 3. (a) SEM image of FG105ACA fiber heat treated at 400 °C for 5 hours; (b) SEM image of FG105ACA fiber before heat treatment; (c) Crystallite growth on FG105ACA fiber at 400 °C and 600 °C

Optical Performance Characterization

To better understand the dominant loss mechanism and related thermal emission the annealing temperature was increased to 1200 ºC and the optical spectra of the low and high OH pure silica core multimode fibers, FG105LCA and FG105UCA, were evaluated in air.

As shown in Fig. 4, there are no "negative loss" peaks, therefore no thermal emission present in the low OH fiber (Fig. 4(a)), but these were evident in the high OH fiber (Fig. 4(b)), which is consistent with the literature and attribution to OH. The spectral features of the low OH fiber consist of an absorption peak at 1390 nm which is attributed to the formation of Si-OH. Conversely, thermal emission peaks at the first two Si-OH overtones, centered at approximately 1240 nm and 1390 nm, were observed for the high OH fiber.

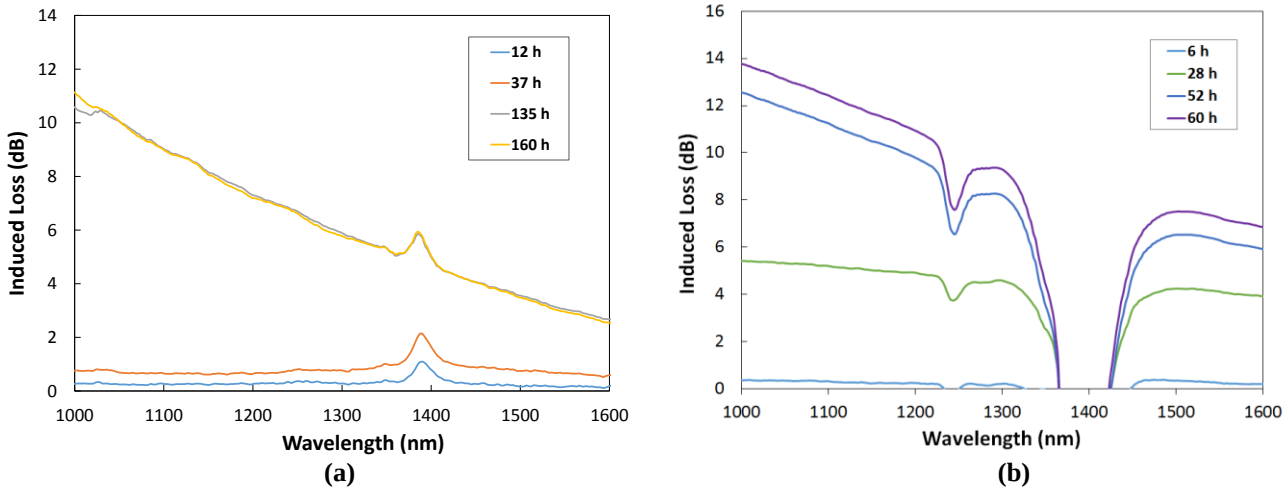

Figure 4. Spectrum of (a) low OH multimode FG105LCA fiber and (b) high OH multimode fiber FG105UCA. ***Please note that the limited dynamic range of the optical spectrum analyzer did not allow for the accurate measurement of the OH overtone centered at ~1390 nm for optical fibers with a relative high OH content.***

Furthermore, a spectrally dependent induced loss that increases with a decrease in wavelength was evident for both fibers, and is consistent with a redistribution of defects in the glass akin to the short wavelength induced edge (SWE) loss, that is prevalent in germanium doped fibers exposed to H_2 at elevated temperatures. At temperatures in excess of 900-1000 °C researchers [12] observed the peroxy linkages (=Si-O-O-Si=) growth, through the reaction of oxygen vacancies and interstitial dioxygen molecules.

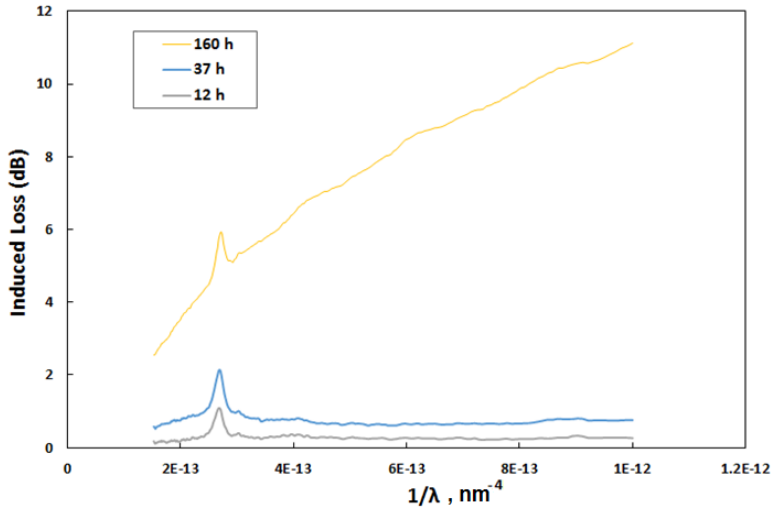

Figure 5. Spectrum of low OH multimode FG105LCA showing λ^{-4} Rayleigh-type attenuation

Surface Characterization

It was expected that defects should be observed on the fiber surface, because significant broadband loss (exceeding 10 dB) was observed for both samples. The SEM images confirmed that significant crystallization took place. The surface of the FG105LCA fiber after long-term heat treatment (55-160 hours) at 1200 °C (shown in Fig. 6 (a)), contains the crystals with diameters larger than those observed at the temperatures 400-600 °C (less than 10 μm comparing to 20-100 μm). From the images with lower magnification it can be seen that a large area of the fiber is affected by crystallization and the larger crystals maintained dendritic morphology. [22] The smaller crystallites have similar to previously shown irregular "bumpy" structure (shown in Figure 6(b)), which is attributed to earlier stages of crystal formation. Figure 6(c) shows the surface of the fiber after 160 hours of heat treatment at 1200 °C.

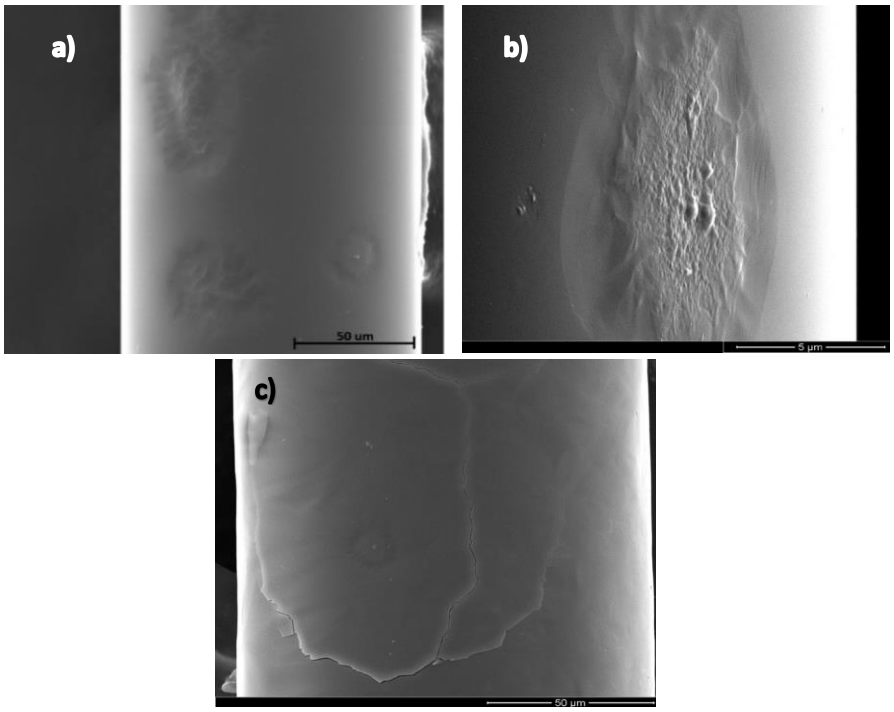

Figure 6. (a) Surface of FG105LCA after a) and b) 55 hours and c) 160 hours of heat-treatment at 1200 °C

The cracks around the crystal areas (Fig. 7) can be observed, and could contribute to the effects seen in the optical spectra.

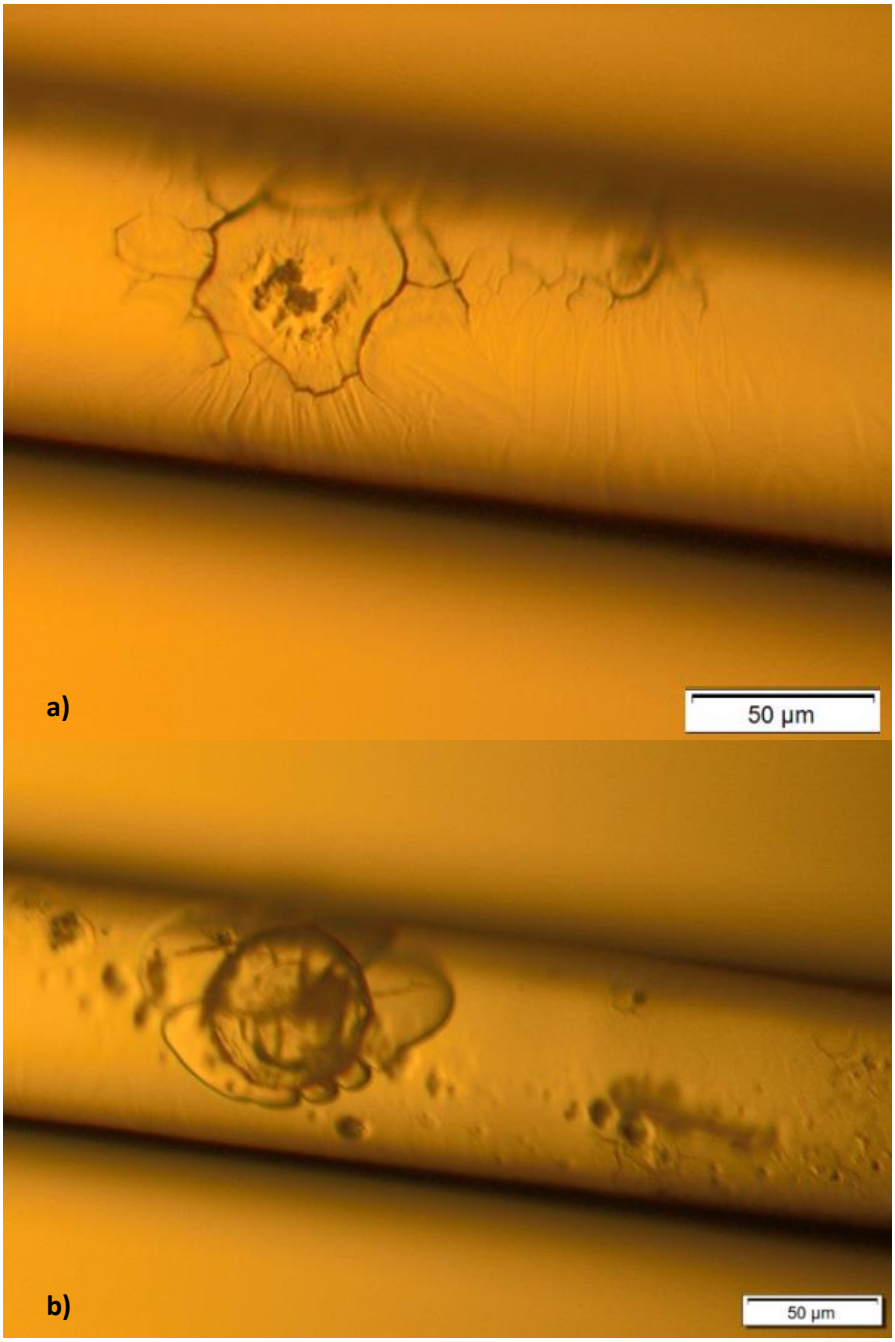

Figure 7. Optical micrograph in reflected light of FG105LCA fiber heat treated in air at 1350°C for 104 hours

Their formation is explained by the coefficient of thermal expansion mismatch [27]. At 1200 °C the thermal expansion coefficients of cristobalite and amorphous SiO_2 are very close, but as the temperature rapidly drops, the coefficient of linear thermal expansion of cristobalite starts growing rapidly ($\alpha \sim 80 \cdot 10^{-7}\ K^{-1}$), while the SiO_2-melt has a very low coefficient of linear thermal expansion ($\sim 5 \cdot 10^{-7}\ K^{-1}$), which results in cracking of the amorphous silica-cristobalite interface region. The cracking is more obvious when fibers are heated up to higher temperatures (optical micrograph of the fiber after 104 hours at 1350 °C (Fig. 7) and after 153 hours at 1350 °C (Fig. 8)).

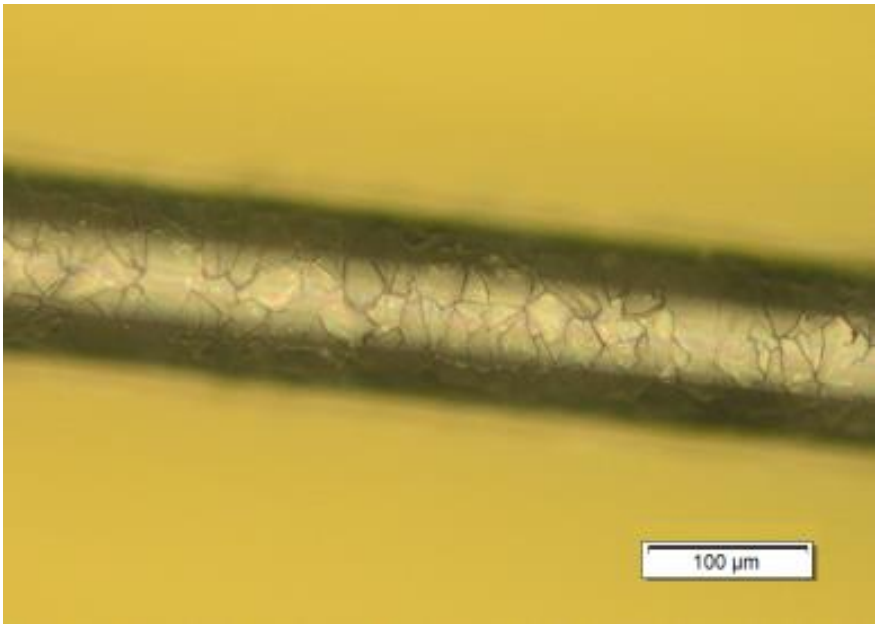

Figure 8. Optical micrograph in reflected light of FG105LCA fiber heat treated in air at 1350 °C for 153 hours

The cracks formed upon cooling are responsible for significant decrease in mechanical performance of the optical fibers. However, even when the temperatures are held above 1200 °C, the mechanical strength of optical fiber can degrade. The formation of cracks as well as stress risers can be associated with the volume contraction related to the formation of cristobalite crystals: the density of cristobalite is in the range of 2.32 - 2.36 g/cm^3 and is higher than the

density of amorphous silica (2.196 g/cm^3). [49]

There are three main low-pressure forms of crystalline SiO_2: quartz, tridymite and cristobalite [23] (the phase diagram is shown in Fig. 9). If cooling through the glass transition temperature is rapid enough to prevent crystallization, the structure is in the form of amorphous SiO_2 silica glass.

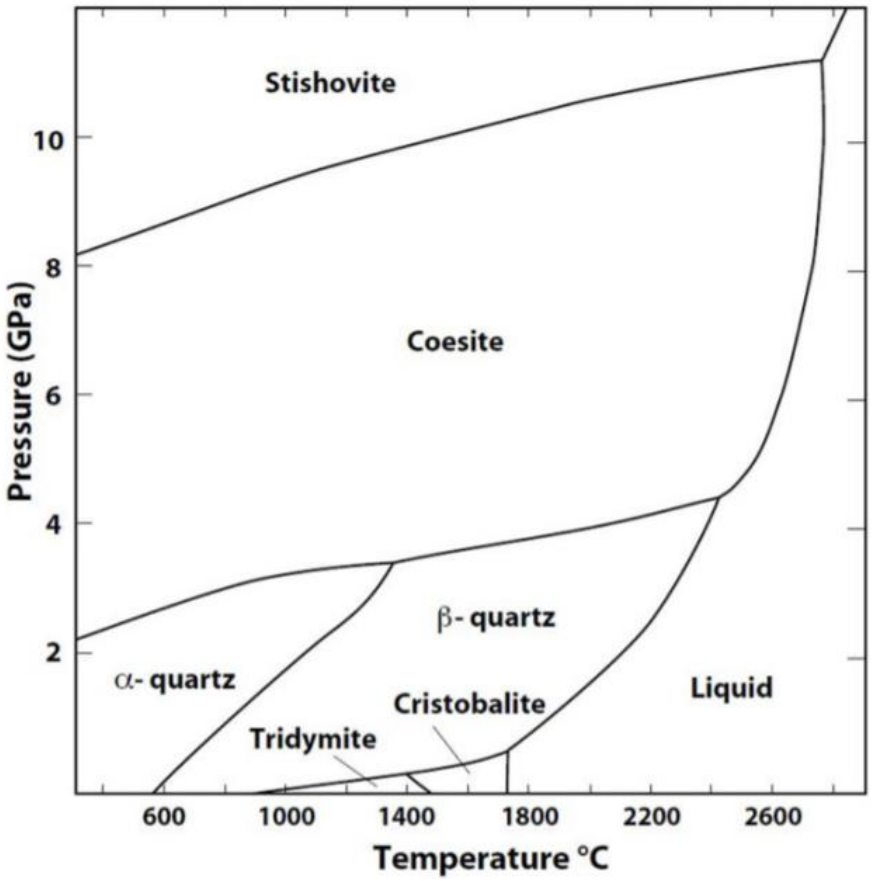

Figure 9. Phase diagram of SiO_2 [23]

Based on the data available in the literature and X-ray diffraction pattern analysis obtained by researchers [24], the similarities in appearance [4][22][24][27] , as well as similar annealing temperatures (500 – 1350 °C), it can be concluded, that the observed crystallites (Figures 6 and 7) are crystals of cristobalite.

Optical microscopy in polarized light

It is well known that optically isotropic media, such as glass, can produce birefringence when deformed, which is the property of a material to have a refractive index that depends on the polarization direction. [26] Stress-induced birefringence has practical application in polarization maintaining fibers, such as PANDA, bow-tie, elliptical clad, where regions of stress are deliberately created during the drawing process to create birefringence and separate out the two polarization modes from cross-coupling.

It is also possible to observe the stress in glass with optical microscopy in polarized light. The samples of the fibers heat treated for longer times (exceeding 60 hours) at higher temperature (1200 ℃ and 1350 °C) and subsequently with larger crystals formed, were investigated under an optical microscope in polarized light in transmission mode (Fig. 10, 11), which makes it possible to observe the induced level of stress: the number of interference fringes is proportional to stress magnitude.

Figure 10 (a) demonstrates the crystal distribution on the surface of the fiber is similar to the one observed under SEM. The crystal morphology cannot be seen in detail as precisely as under SEM due to the lower resolution of the optical microscope, however the same dendritic features (Figure 9(a)) and irregular “bumpy” pattern is observed.

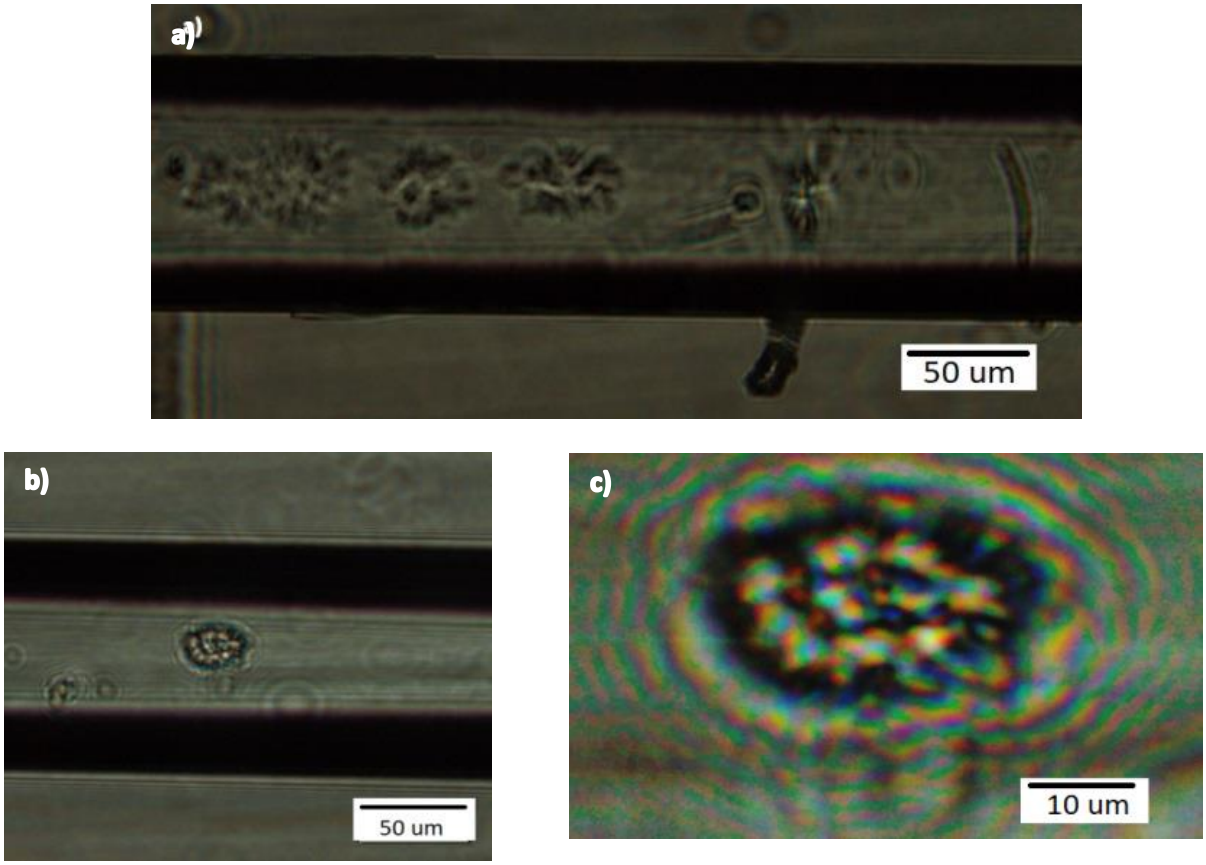

Figure 10 Optical micrographs of (a) FG105UCA fiber after 160 hours and (b, c) FG105LCA fiber after 135 hours at 1200 °C

As it has been mentioned earlier, cristobalite crystals within the amorphous silica glass can decrease the mechanical performance by acting as stress risers. The stress can form upon cooling due to small thermal expansion mismatch between the cristobalite and amorphous silica [27]

The optical polariscope scheme includes polarizer and analyzer (second polarizer, rotated 90° relatively to the polarizer) in its optical pathway. When the birefringent sample (glass with stress region) is placed in this pathway, it produces two individual wave components (ordinary and extraordinary wave), that are then recombined at the analyzer, producing constructive and destructive interference, the amplitude of the light will be described as follows:

$$A = a\ sin\alpha \cos\alpha \cos\omega t \sin\frac{\Delta}{2} \quad (2)$$

Where α is the angle between one transmitted wave and the polarizer axis, and Δ is a phase shift of the two transmitted waves due to their different transmission velocities in the stressed model.

The number of fringes, which is proportional to the phase shift is:

$$N = \frac{\Delta}{2\pi} \quad (3)$$

Which in turn is proportional to the principal stress that causes the birefringence:

$$\sigma = Nf_2/h \quad (4)$$

Where h is the thickness of the birefringent region and f_2 is fringe stress coefficient, that is equal to λ/c≈157 kN/m for the silica glass. The isochromatic fringe order can be identified using the color chart in [40], and the stress can be estimated using formula (4) to be around *~0.75 GPa.*

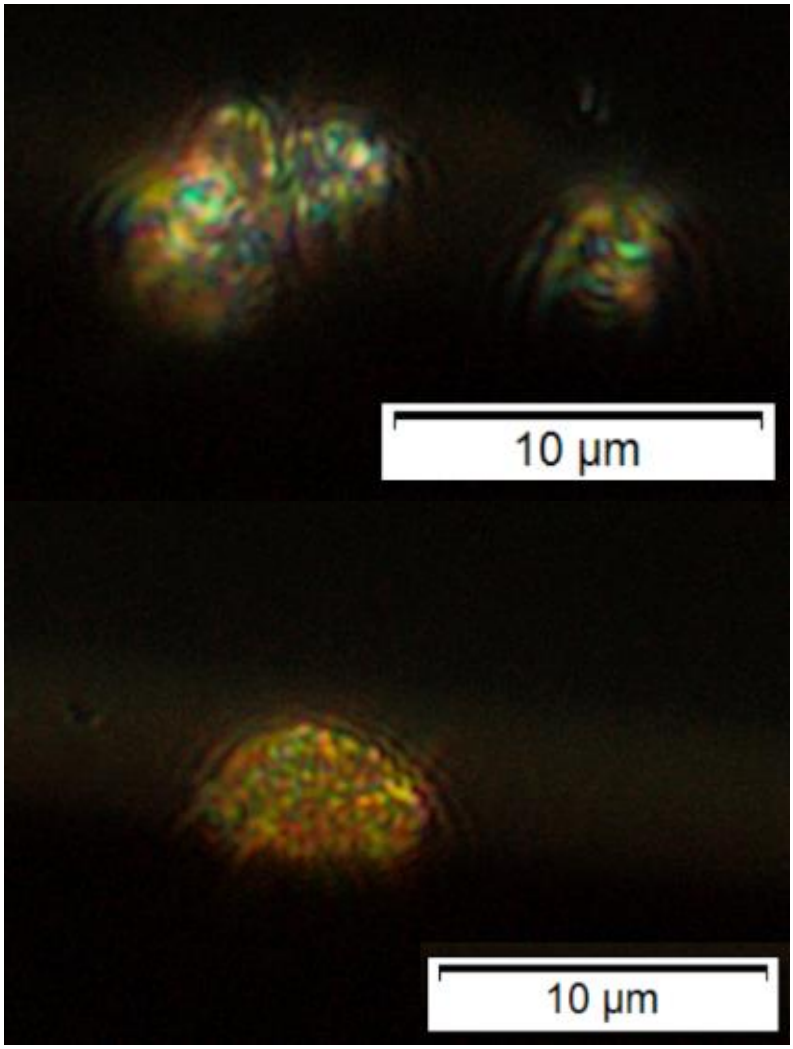

Figure 11. Dark field optical micrograph in polarized light of FG105LCA heat treated at 1350°C for 60 hours

From the figure above it is possible to qualitatively examine the stress in amorphous silica surrounding the cristobalite. As the cristobalite shrinks more rapidly upon cooling than does the surrounding amorphous silica, the tensile stresses across the glass-crystal boundary are generated and are apparent in Fig. 6c and Fig. 7, radially propagating from the crystal. Using the Eshelby model for a hemispherical inclusion [32], the stress inside the cristobalite inclusion is uniform tension that can be expressed as [27]:

$$\frac{2E(\alpha_m - \alpha_p)\Delta T}{3 - 3\upsilon} = \sigma_r^{(p)}$$

where E is the elastic modulus, α refers to the coefficient of thermal expansion of the amorphous silica and crystal of cristobalite respectively, and ΔT is the change in temperature and υ is Poisson ratio, and the σ_r is the stress in the glass matrix (radial tension) surrounding the crystal. To estimate the residual stress levels, the parameters for fused silica glass available in the literature were picked [36]: Young's modulus $E = 70\ GPa$, Poisson ratio $\upsilon = 0.17$ and coefficient of thermal expansion $\alpha_m = 5\ 10^{-7}\ °C^{-1}$; and the coefficient of thermal expansion for cristobalite $\alpha_m = 80\ 10^{-7}\ °C^{-1}$. The estimated residual stress is in the order of $\sigma \sim 0.5$ GPa, which is in a good agreement with the data obtained with the polariscope. The data available in the literature for the internal residual stresses in glass-ceramics is in the range of 0.03 – 1 GPa. [37]

Cross-Section Characterization

By taking images of the cross-sections of the optical fibers after heat treatment, it is possible to determine the extent of penetration of the crystals from the surface and to address whether the crystals are also forming in the bulk of the fiber.

The decoated optical fibers with the crystals formed on the surface are extremely fragile, and it is hard to achieve a smooth cleave or polishing results. The fiber cross-sections shown in the Fig. 13, 14 have multiple fractures and the defects, resulting from decreased mechanical strength. However, it is still possible to examine for the presence of crystals in the bulk, not taking into account the fractures that result from cleaving the fiber. The multimode fibers (FG105LCA and FG105UCA), heat treated at 1350 °C in air for 60-176 hours, were cleaved and investigated with optical microscopy in reflected light and transmitted light with crossed polarizers.

Researchers have shown [33] that the surface crystallization dominates over internal crystallization, which is only present when there are defects (such as impurities or flaws) within the glass matrix, and there are always dust particles and scratches on the surface from the surrounding environment that can serve as nucleation sites for the crystallization process. To confirm that there were no internally nucleated crystals, the fiber cross sections were investigated in transmitted light with crossed polarizers, and as it can be seen in the Fig. 12, there are no illumination regions.

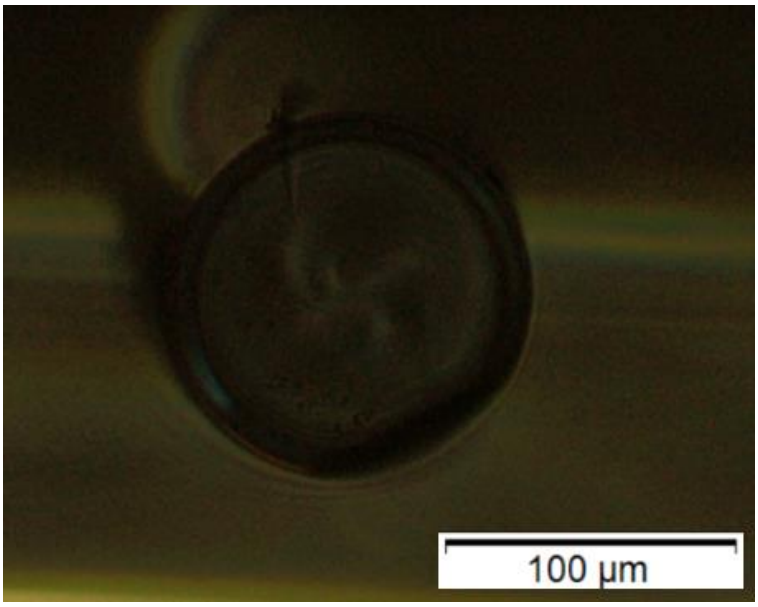

Figure 12. Cross section of FG105UCA heat-treated at 1350°C in air for 60 hours

The cross sections of multimode fibers FG105LCA and FG105UCA with low and high OH content respectively were investigated, and the optical microscopy images with various heat-treatment times at 1350 ℃ are shown in Fig. 13 and 14 respectively. It is observed, that the high OH fiber's crystals have more non-uniform front, and a larger thickness (18 - 41 μm) that is formed compared to the crystals formed in low OH fibers (with the thickness of 5 - 30 μm). This can be explained by regarding the OH content as an impurity [41], as well as considering the fact that the influence of the OH-content on internal friction in the glass transition range is closely connected to the viscosity, which is lowered considerably by the incorporation of OH-groups.

The measured thickness of the crystallized layer of the cross sections is in the range of 5 - 41 um. In the paper [33] the thickness of the crystallized layer was measured with SHG microscopy and optical microscopy of the cut section, and it was estimated to be around 14 um (after 3 hours in air at 1100 ℃), which is in the range of the measurement of this experiment.

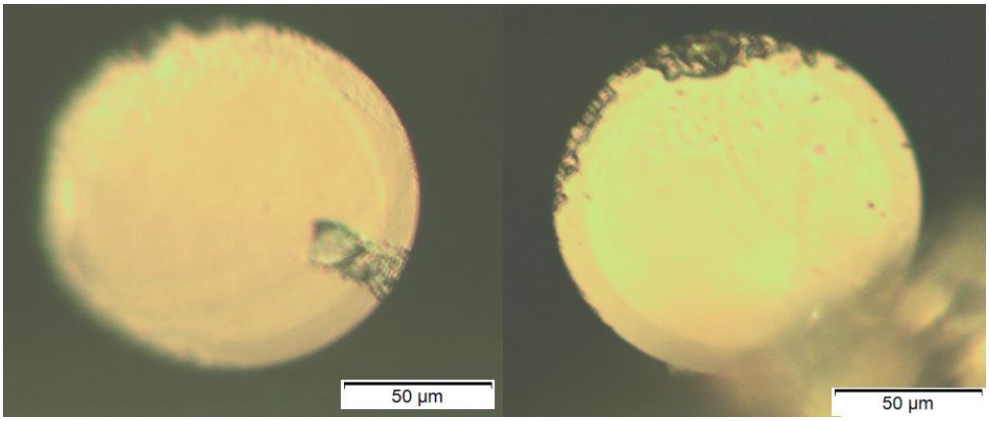

a) b)

Figure 13. Cross-section images of FG105LCA heat treated in air at 1350°C a) for 104 hrs and b) for 132 hrs

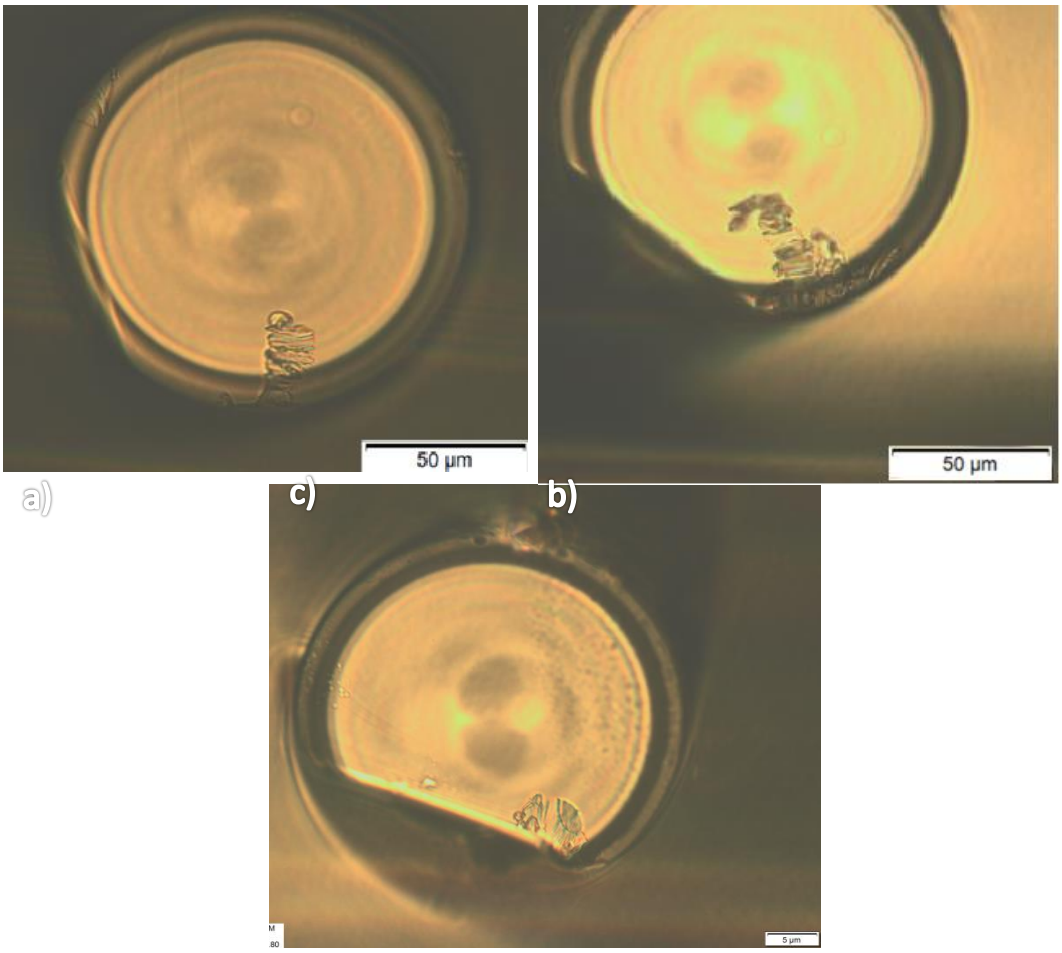

Figure 14. Cross-section images of FG105UCA heat treated in air at 1350 °C for 60, 132 and 176 hours

The stressed region of the glass, which is described in detail in the previous chapter, is also obvious in the cross section images (illuminated area). The dark field image taken in transmitted polarized light with crossed polarizers of FG105LCA heat treated at 1350 °C for 104 hours is shown in Fig. 15.

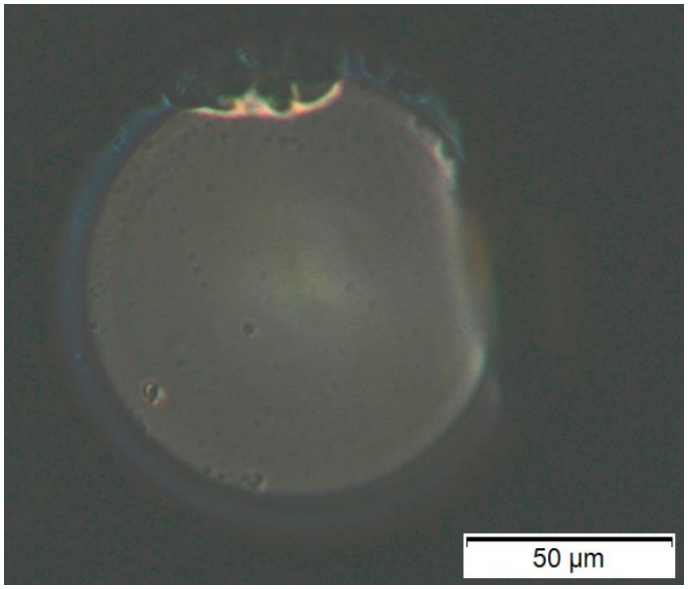

Figure 15. Cross section of FG105LCA heat-treated at 1350 °C in air for 104 hours

Crystallization Kinetics

Crystallization in glass has been widely studied in the bulk for different types of silica. [15][16] By measuring the growth as a function of time for several temperatures it is possible to estimate the activation energy of crystallization (the minimum energy required to start the reaction). [17][18]

There are two main mechanisms for nucleation: homogeneous and heterogeneous. Nucleation without preferential nucleation sites is homogeneous nucleation, it occurs spontaneously and randomly. Heterogeneous nucleation forms at preferential sites such as phase boundaries, surfaces or impurity particles. At such preferential sites, the effective surface energy is lower, and therefore, it diminishes the free energy barrier and facilitates nucleation. [43]

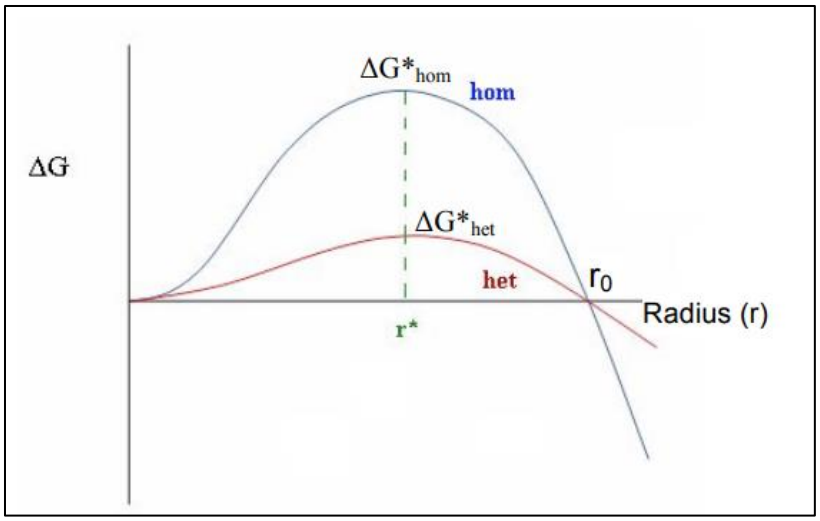

Figure 16. Free energy barrier as a function of radius for the cases of homogenious and heterogeneous nucleation. [43]

Heterogeneous nucleation is the main mechanism to transform pure silica glass into cristobalite as the only modification, as it has been proven by the researchers. [44] Impurity

centers, flaws, scratches, surface tips and edges, present in the glass can serve as the heterogeneities. [33] In the current experiment, the environmental conditions were not controlled (heat treatment was performed in ambient air, without vacuum, or high pressure gas), therefore, the contaminations such as dust and alumina particles, were present, and the heterogeneous nucleation is assumed.

Crystal growth in silica glasses is controlled by atomic or molecular rearrangements at the crystal-liquid interface, described by the normal model: only a fraction of sites at the glass - crystal interface is available for growth, and this fraction is a function of temperature. [24] The atomic or molecular attachment at the interface is defined by effective diffusion coefficient, that is inversely proportional to the viscosity. The studies [34] [35] showed that the growth rate of cristobalite is related to the viscosity of silica

$$\mu = \frac{\Delta h\ (T_m - T)}{3\pi a^2 \eta T_m} \tag{3}$$

and therefore has the same temperature dependence:

$$\eta = \eta_0 \exp(\frac{E_A}{RT}) \tag{4}$$

where η is viscosity, μ is crystal growth rate equation, Δh is the heat of fusion per molecule, T_m is the melting temperature, and a is the jump distance.

The plot $log(\mu/(T_m - T))$ vs $1/T$ will have a slope that is equal to E_A/R. Therefore, by measuring the crystal diameters as a function of time at different temperatures approaching glass transition temperatures, it is possible to estimate the activation energy of crystallization.

Crystal growth rates of the studied optical fibers (multimode fibers with low and high relative OH content: FG105LCA and FG105UCA) were obtained by measuring the crystal diameter. Most crystals had uniform circular shape, as shown in the previous chapters. Several samples were heated up to 1100, 1200 and 1350°C and pulled out of the furnace at specified times, then the average diameters of the crystals formed on these samples, along with the standard deviation, were plotted, as shown below (in Fig. 17).

To determine the mechanism of growth, which is the manner in which atoms or molecular groups attach to the growing crystal surface, in the case of silica and silica-based systems, it is necessary to obtain the system's kinetics, in this case the crystal growth rates at undercooling temperatures. This linear relationship (Fig. 17) with time indicates that the growth is interface-controlled: [16] the mechanism that does not involve a change in composition, but only interface motion, and the kinetics involve local atomic rearrangements.

The growth lines in the figure above (dashed) are the linear fit found by the least squares method in Microsoft Excel software.

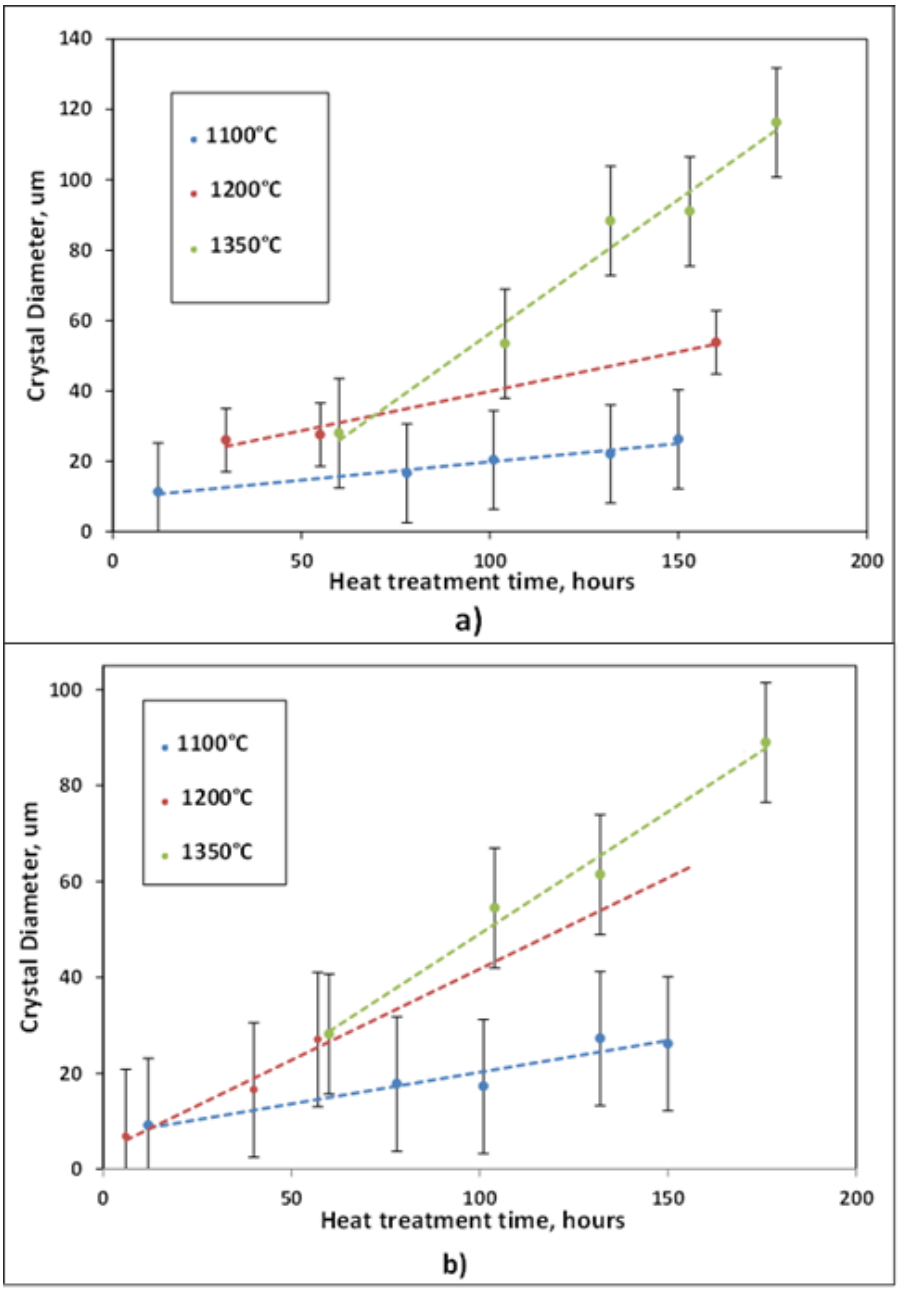

Figure 17. Crystal diameters as functions of time on the fiber surface heat treated at 1100°C and 1200° Cfor a) FG105LCA and b) FG105UCA

The crystal growth rate (μ) is the slope of the curves above, and as expected, it is larger at higher temperatures. Then, according to Equation 3 and 4, by plotting the natural logarithm of the crystal growth rate as a function of inverse temperature (T), the activation energy can be obtained. Arrhenius plots for the crystallization of optical fiber surfaces are shown in Fig. 18.

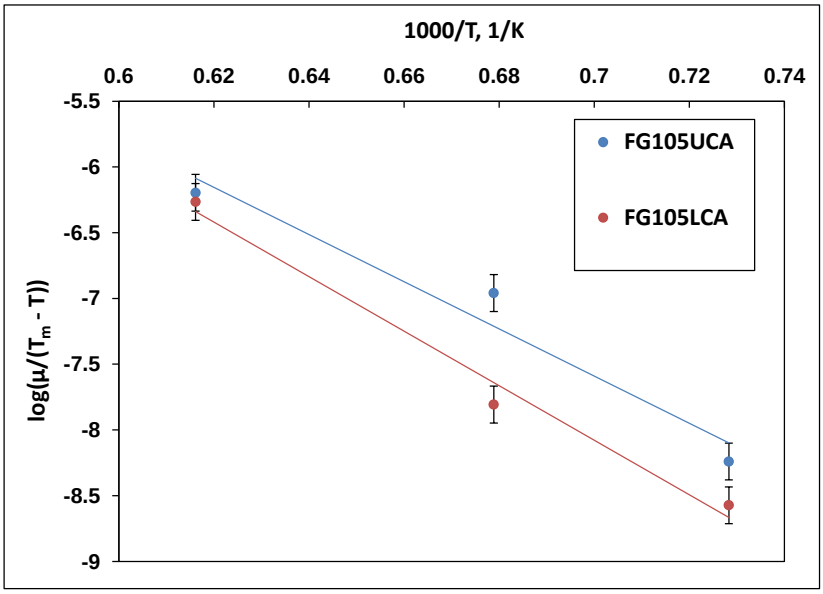

Figure 18. Arrhenius plots for the crystallization of optical fiber surfaces

Therefore, according to Equation 4, the slopes of the dependences in the figure above are E_A/k_B. The estimated activation energy of crystallization of the fused silica cladding of FG105UCA fiber is E_A=149.2 kJ/mol and of FG105LCA is E_A=175.6 kJ/mol. These values are approximately 70kJ/mol lower than measured by some other researchers [22]: 239 – 348 kJ/mol.

These values could have been affected by various parameters, such as different surface conditions (presence of scratches and flaws), environmental testing conditions (uncontrollable presence of alumina particles from furnace isolation), as well as different glass composition: the optical fibers used in this study had fluorine-doped cladding, and it has been reported that the viscosity decreases with an increase of the fluorine content in glass [48], and therefore, the crystal growth is promoted. The optical fiber geometry and manufacturing methods also effect the properties such as fictive temperature, that directly affects the peculiarities of crystallization. [50] Moreover, as expected, high OH content glass has lower activation energy, as the OH breaks the Si-OH bonds and lowers the viscosity.

The estimated activation energies relied on the mean value and standard deviation while calculating the linear regression of crystal growth with time at each temperature. It appears that the slope at each temperature for low OH content fiber (FG105LCA) is steeper than for high OH content fiber (FG105UCA) at the same temperature. However, it needs to be proved with statistical methods that there is in fact significant difference in slopes.

The Table 4 below demonstrates the calculations of t-test (for 1100°C, 1200°C and 1350°C), and based on pooled and unpooled values for s_{Res}, the null hypothesis, H_0, that states that the slopes are equal, cannot be rejected [25].

1100°C	**UCA**	**LCA**
n	39	62
b	0.126188	0.104548
Sy.x	11.53292	10.64714
Sx	45.73331	50.42844
Sb	0.040909	0.027033
	Unpooled error variance	Pooled error variance
Sres2		120.8557
Sb1-b2	0.049034	0.047955
t	0.441329	0.451254
df	97	97
a	0.05	0.05
p-value	0.659957	0.652814
t-crit	1.984723	1.984723
sig	no	no
1200°C	**UCA**	**LCA**
n	33	22
b	0.379874	0.224872
Sy.x	5.580307	13.85433
Sx	18.10876	44.03963
Sb	0.176777	0.068649
	Unpooled error variance	Pooled error variance
Sres2		94.19968
Sb1-b2	0.189638	0.106253
t	0.817354	1.458801
df	51	51

a	0.05	0.05
p-value	0.351518	0.150752
t-crit	2.007584	2.007584
sig	no	no
1350°C	**LCA**	**UCA**
n	51	54
b	0.687079	0.506178
Sy.x	29.93896	28.1098
Sx	44.1331	39.6432
Sb	0.095937	0.097398
	Unpooled error variance	Pooled error variance
Sres2		841.6741
Sb1-b2	0.853401	0.136921
t	0.211977	1.321204
df	101	101
a	0.05	0.05
p-value	0.832552	0.189419
t-crit	1.983731	1.983731
sig	no	no

Table 4. t-test to compare slopes of regression lines

Furthermore, using the uncertainty of the slope Sb calculated above, the uncertainty of the slope of the fit of Arhenius plots (Figure 18) can be calculated (Table 4). That gives the uncertainty of the activation energy: for FG105LCA the confidence interval is ±23.94 kJ/mol and for FG105UCA it is ±32.41 kJ/mol. Therefore, it cannot be concluded with statistical confidence, that the activation energy of crystallization of high OH optical fiber is in fact lower than low OH, however, the mean values, along with theoretical and experimental results obtained the other researchers, confirm the influence the OH content in silica on crystallization.

	UCA	LCA
n	3	3
b	-17.9518	-21.1298
Syx	0.310116	0.221005
Sx	0.056226	0.054235
Sb	3.900075	2.881432

Table 5. t-test to compare slopes of regression lines

HEAT TREATMENT IN WATER VAPOR ATMOSPHERE

Prior studies of fused silica glass in bulk and optical fiber, have shown that water vapor at elevated temperatures (500 ℃ and above) induces crystallization by breaking of silicon-oxygen bonds in the glass matrix [16] and this forms hydroxyl groups with characteristic absorption peaks in the infrared [7].

In an effort to better characterize the growth of the first Si-OH overtone centered at 1390 nm, the performance of a traditional single mode fiber was evaluated upon exposure to a nitrogen with water vapor atmosphere at 1000 °C.

The features in the induced attenuation spectra (the spectra was obtained as the difference between the recorded spectra and the baseline measurement at room temperature in air) for the single mode fiber exposed to ambient air at 1200 ºC, as shown in Fig. 19. (a) are consistent with those observed in the low OH pure silica core multimode fiber.

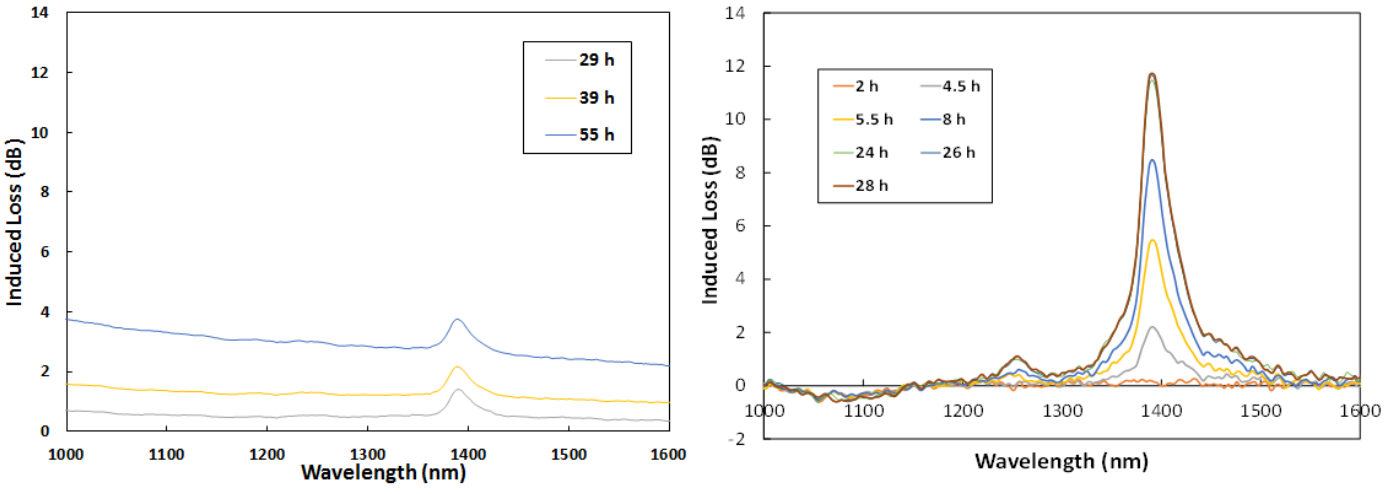

(a) **(b)**

Figure 19. (a) Spectrum of single mode Spectran fiber heat treated at 1200°C for 55 hrs. in ambient air and (b) 1000°C for 28 hours in water vapor atmosphere

The hydroxyl absorption peak (Fig. 19(b)), centered at 1390 nm, initially grew but quickly slowed or ceased (can be seen in Fig. 20), that is associated with the limit of physical solubility for molecular hydrogen in fused silica glass of the optical fiber. [45]

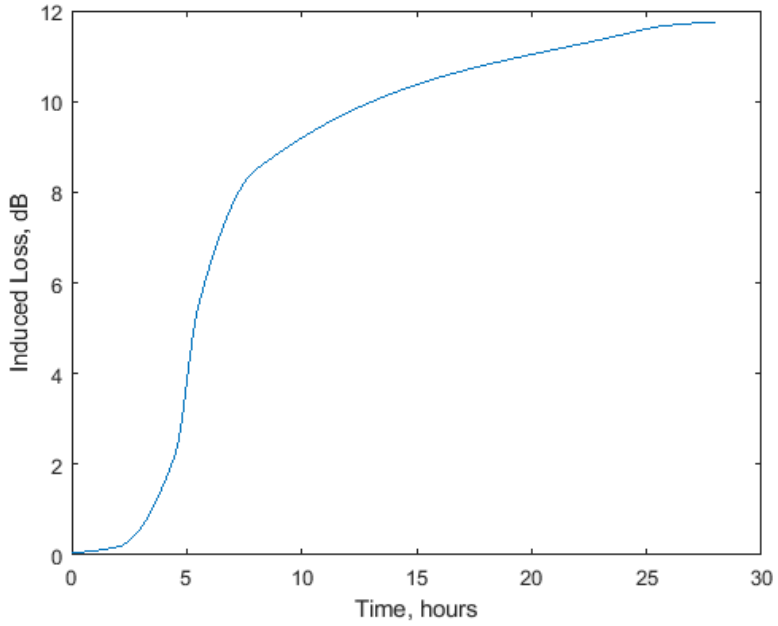

Figure 20. Induced loss at 1390 nm in Spectran SMF fiber at 1000°C

In comparison to the heat treatment in ambient air (Figure 19), the growth of the OH peak was significant upon exposure to water vapor due to the formation of Si-OH.

After investigating the surface of the fiber under SEM it was observed that after 22 hours of heat treatment at 900 °C in water vapor atmosphere (Figure 21 and Figure 22) a significant amount of the surface is crystallized. Crystals changed their circular shapes and merged, covering the fiber surface. Therefore, it became impossible to measure separate crystal diameters.

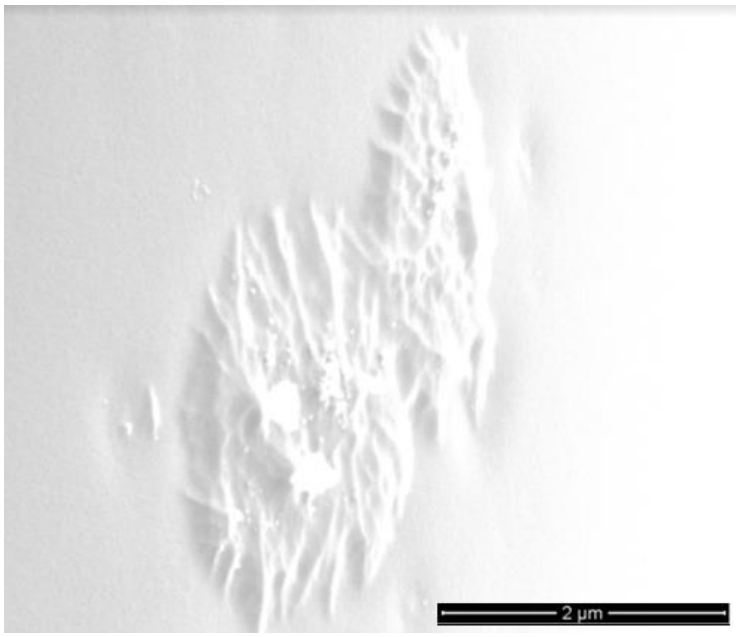

Figure 21. SEM image of the crystals formed on the surface of Spectran SMF after 22 hours of heat treatment at 900°C in water vapor atmosphere

The activation energy of crystallization in the presence of water vapor was calculated using the method described in the previous chapter. To estimate the extent of crystallization at each time, the percent of surface crystallized was measured using ImageJ, as shown in Fig. 21, and then plotted as a function of time. The slopes of these functions give the rate constants (*k*).

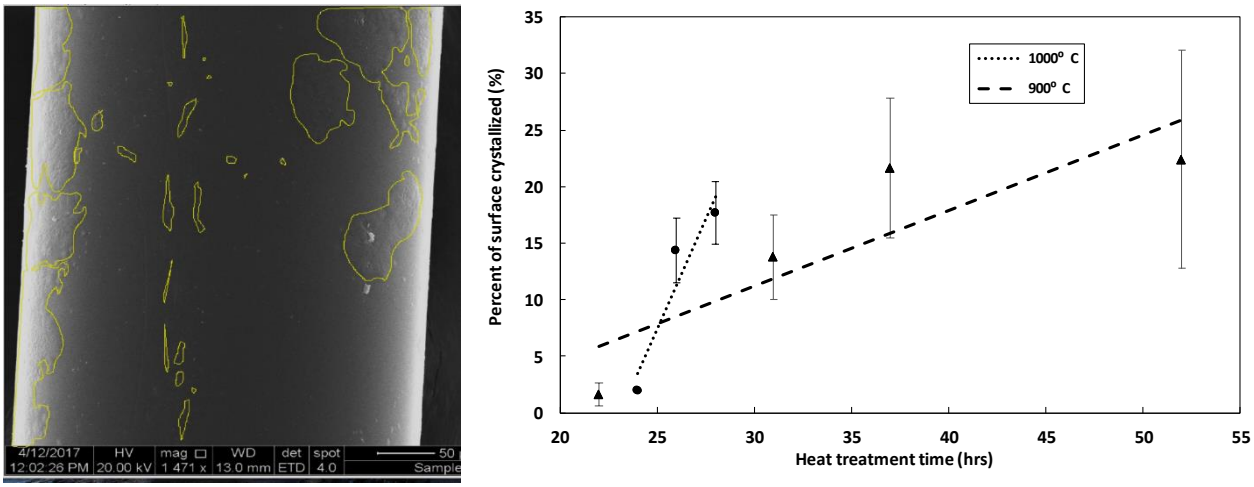

Figure 22. Percent of fiber surface crystallized as a function of heat treatment time in water vapor atmosphere

Arrhenius plot for the crystallization of the surface of Spectran SMF is shown in Fig. 23. The estimated activation energy is E_A=102.3 kJ/mol. The confidence interval, calculated using the same method as in the previous chapter, is ±13.4 kJ

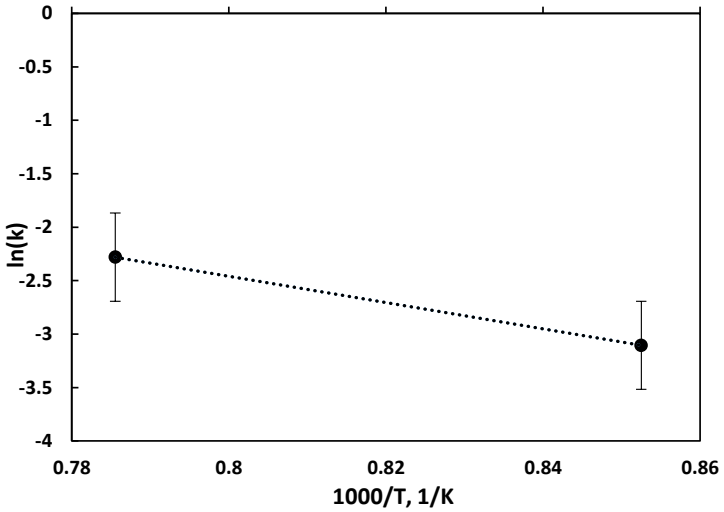

Figure 23. Arrhenius plots for the crystallization of Spectran SMF surface in the presence of water vapor

It was expected, based on the literature, that the presence of water vapor decreases the activation energy through introducing OH in the glass, that breaks the silicon-oxygen bonds and decreases the viscosity of the amorphous silica. This was confirmed in the current study: the activation energies in ambient air are E_A=149.2 kJ/mol and E_A=175.6 kJ/mol compared to E_A = 102.3 kJ/mol.

CONCLUSIONS

Crystal growth was observed on the surface of commercial fused silica optical fibers at high temperatures (400 °C – 1200 °C).

The crystallites formed at different heat treatment times and temperatures were characterized with SEM and optical microscopy: their growth with time was observed and it was shown that it is faster at higher temperatures. The activation energies of crystallization for High OH and Low OH multimode fibers were estimated to be E_A=175.68 kJ/mol and E_A=149.2 kJ/mol respectively, and activation energy of crystallization in the presence of water vapor of Spectran single mode fiber was found to be E_A=102.3 kJ/mol. Due to large variance in the crystal sizes at each point of time, the confidence intervals of these values are large, and therefore it cannot be concluded with statistical confidence from these experiments that the presence of water vapor or the increased content of OH in silica glass promotes or retards the nucleation or crystal growth process. However, even with some uncertainty, these calculations can give a confirmation, that the presence of OH either from the atmosphere or the contents of the glass, induces the crystallization to occur more easily, based on the lower values of activation energy, and this data can be used while selecting optical fibers for high temperature applications.

The optical performance of the fibers was monitored at different stages of crystal growth: optical transmittance seems to be affected at temperatures in excess of 1200°C even in as little as 6 hours, or at lower temperatures (1000 °C) after 4 hours with the presence of water. Therefore, it can be concluded that multimode High OH and Low OH fibers (FG105UCA and FG104LCA) can be used at temperatures up to 1000°C depending upon the length of time and water content in the atmosphere: no effects in the optical spectrum were observed, as well as no broadband loss

for the long-term duration of the tests (over 200 hours). However, the decreased mechanical performance should be accounted for, as the crystallites form even at low temperatures (400 °C).

For the future work, it is suggested to further extend the data base of commercially available fibers and environmental conditions such as different gaseous species, pressure, temperature ranges; investigate the coating degradation at elevated temperatures, and perform the mechanical testing of the crystallized optical fibers. The knowledge of spectral effects at elevated temperatures such as thermal emission peaks, absorption bands, and short wavelength induced edge (SWE) is limited and should also be further investigated.

References

[1] U. S. Department of Energy, "'Strategic Plan 2014-2018.,'" *DOE/CF-0067*, 2014.

[2] P. R. Ohodnicki, Jr., "Embedded Sensors for Extreme Temperature and Harsh Environments," *NETL-RUA Commer. Oppor. Summ.*, 2013.

[3] A. Azad, C. Holt, and S. Swartz, "Development of chemical sensors for PEM and SOFC systems," *Fuel Cells Secur. Sustain. Energy Abstr.*, 2003.

[4] U.S. Department of Energy, "Technical Readiness and Gaps Analysis of Commercial Optical Materials and Measurement Systems for Advanced Small Modular Reactors," no. August, 2013.

[5] D. Tosi, S. Poeggel, G. Leen, and E. Lewis, "Adaptive filter-based interrogation of high-sensitivity fiber optic Fabry-Perot interferometry sensors," *Sensors Actuators, A Phys.*, vol. 206, pp. 144–150, 2014.

[6] S. J. Mihailov, D. Grobnic, R. B. Walker, P. Lu, and H. Ding, "Femtosecond laser induced optical fiber Bragg gratings (FBGs) for harsh environment sensing applications," *2015 IEEE Photonics Conf.*, vol. 2, pp. 339–340, 2015.

[7] B. Liu, Z. Yu, C. Hill, Y. Cheng, D. Homa, G. Pickrell, et al., "Sapphire-fiber-based distributed high-temperature sensing system," Optics Letters, vol. 41, pp. 4405-4408, 2016.

[8] G. Coviello, V. Finazzi, J. Villatoro, and V. Pruneri, "Thermally stabilized PCF-based sensor for temperature measurements up to 1000 degrees C.," *Opt. Express*, vol. 17, no. 24, pp. 21551–9, 2009.

[9] A. H. Rose, "Devitrification in annealed optical fiber," *J. Light. Technol.*, vol. 15, no. 5, pp. 808–814, 1997.

[10] A. H. Rose and T. J. Bruno, "The observation of OH in annealed optical fiber," *J. Non. Cryst. Solids*, vol. 231, no. 3, pp. 280–285, 1998

[11] Mulrooney, Jim, John Clifford, Colin Fitzpatrick and Elfed Lewis. "Detection of Carbon Dioxide Emissions from a Diesel Engine Using a Mid-Infrared Optical Fibre Based Sensor." Sensors and Actuators A: Physical 136, no. 1 (2007): 104-110.

[12] Nishikawa, H., R. Tohmon, Y. Ohki, K. Nagasawa and Y. Hama (1989). "Defects and optical absorption bands induced by surplus oxygen in high purity synthetic silica." Journal of Applied Physics 65(12): 4672-4678.

[13] L. Yu *et al.*, "Observation of temperature dependence of the IR hydroxyl absorption bands in silica optical fiber," *Opt. Fiber Technol.*, vol. 30, pp. 1–7, 2016.

[14] F. Li, "Study of Stress Measurement Using Polariscop e Study of Stress Measurement Using Polariscope," no. August, 2010.

[15] K. Thieme, I. Avramov, and C. Rüssel, "The mechanism of deceleration of nucleation and crystal growth by the small addition of transition metals to lithium disilicate glasses," *Nat. Sci. Reports*, no. May, pp. 1–16, 2016.

[16] F. E. Wagstaff and K. J. Richards, "Kinetics of Crystallization of Stoichiometric SiO2 Glass in H_20 Atmospheres," *J. Am. Ceram. Soc.*, vol. 49, no. 3, pp. 118–121, 1965.

[17] Nascimento, M. L. F. & Zanotto, E. D. Diffusion processes in vitreous silica revisited. Phys. Chem. Glasses-Eur. J. Glass Sci. Technol. B 48 201–217 (2007).

[18] Rahul Vaish and K B R Varma The glass transition and crystallization kinetic studies on $BaNaB_9O_{15}$ glasses Journal of Physics D: Applied Physics, Volume 42, Number 1(2008)

[19] K. Thieme, I. Avramov, and C. Rüssel, "The mechanism of deceleration of nucleation and crystal growth by the small addition of transition metals to lithium disilicate glasses.," *Nat. Sci. Reports*, vol. 6, no. January, p. 25451, 2016.

[20] Li, Hong, Minoru Tomozawa and Victor K Lou. "Effects of Nitrogen and Carbon Ion Implantation on Devitrification of Silica Glasses." Journal of non-crystalline solids 168, no. 1 (1994): 56-63.

[21] Skuja, Linards. "Optically Active Oxygen-Deficiency-Related Centers in Amorphous Silicon Dioxide." Journal of Non-Crystalline Solids 239, no. 1 (1998): 16-48.

[22] P. J. Lezzi, E. E. Evke, E. M. Aaldenberg, and M. Tomozawa, “Surface Crystallization and Water Diffusion of Silica Glass Fibers: Causes of Mechanical Strength Degradation,” *J. Am. Ceram. Soc.*, vol. 98, no. 8, pp. 2411–2421, 2015.

[23] C. Koike et al., “Infrared spectra of silica polymorphs,” Proc. Sci., vol. 60, 2013.

[24] F. E. Wagstaff, “Crystallization Kinetics of Internally Nucleated Vitreous Silica,” J. Am. Ceram. Soc., vol. 51, no. 8, pp. 449–453, 1968.

[25] Zaiontz C. (2018) Real Statistics Using Excel. www.real-statistics.com

[26] R. Ulrich, Polarization and Birefringence Effects. Academic Press, Inc., 1994.

[27] R. C. Breneman and J. W. Halloran, “Stress Development and Fracture of Surface Nucleated Cristobalite on Silica Glass,” J. Am. Ceram. Soc., vol. 97, no. 11, pp. 3483–3488, 2014.

[28] A. Honda, K. Toh, S. Nagata, B. Tsuchiya, and T. Shikama, “Effect of temperature and irradiation on fused silica optical fiber for temperature measurement,” J. Nucl. Mater., 2007.

[29] Yukihiro Yokomachi, Ryoichi Tohmon, Kaya Nagasawa, “Hydrogen Bond of OH-Groups in Silica Glass and its Relation to the 1.39 um Absorption,” J. Non. Cryst. Solids, vol. 96, pp. 663–670, 1987.

[30] M. Tachikura and T. Haibara, “Devitrification Effect on Optical-Fiber Strength Reduction by Fusion Splicing,” J. Light. Technol., vol. 3, no. 3, pp. 662–668, 1985.

[31] Y. Zheng and S. Wang, “Effect of moderately high temperature heat treatment on surface morphology and structure of quartz fibers,” Appl. Surf. Sci., vol. 258, no. 10, pp. 4698–4701, 2012.

[32] D. Eshelby, “The Determination of the Elastic Field of an Ellipsoidal Inclusion, and Related Problems,” Proc. R. Soc. A-Math. Phys. Eng. Sci, 241 [1226] 376–96 (1957).

[33] Honglin An, Ying Tang, Pam McNamara, Simon Fleming, “Characterization of surface

crystallization in Ge-doped graded-index silica glass", Vol. 12, No. 6 OPTICS EXPRESS 1055 (2004).

[34] G. Hetherington, K. H. Jack, and J. C. Kennedy, "Viscosity of Vitreous Silica," Phys. Chem. Glasses, 5 [5] 130-36 (1964).

[35] N. G. Ainslie. C. R. Morelock. and D. Turnbull, Devitrification kinetics of fused silica, in Symposium on Nucleation and' Crystallization in Glasses and Melts. Edited by M. K. Reser, Geraldine Smith, and Herbert Insley. American Ceramic Society, Inc., Columbus, Ohio, 1962.

[36] William N. Sharpe Handbook of Experimental Solid Mechanics, Springer New York, 2008.

[37] F.C. Serbena, E.D. Zanotto, Internal residual stresses in glass-ceramics: A review, J. Non-Cryst. Solids (2012)

[38] Schmelzer, Jürn. Glass: Selected properties and crystallization. (2014)

[39] A. W. Snyder and J. D. Love, Optical Waveguide Theory, Chapman and Hall, London (1983)

[40] A. Ajovalasit, G. Petrucci, M. Scafidi, Review of RGB photoelasticity Optics and Lasers in Engineering Volume 68, pp. 58-73, (2015)

[41] R. Bruckner Properties and structure of vitreous silica. I Journal of non-crystalline solids 5 (1970) 123—175

[42] Handerek V. (1995) Single mode optical fiber sensors. In: Grattan K.T.V., Meggitt B.T. (eds) Optical Fiber Sensor Technology. Optical and Quantum Electronics Series, vol 1. Springer, Dordrecht

[43] Ling Zang (2017) MSE6034 - Kinetics, Lecture notes.
Retrieved from http://www.eng.utah.edu/~lzang/images/lecture-10.pdf

[44] R. Muller, E.D. Zanotto, V.M. Fokin Surface crystallization of silicate glasses: nucleation sites and kinetics Journal of Non-Crystalline Solids 274 (2000) 208-231

[45] Kazuhiro Noguchi, Nor Shibata, Naoshi Uesugi, Yukiyasu Negishi Loss Increase for Optical Fibers Exposed to Hydrogen Atmosphere Journal of Lightwave Technology, Vol. LT-3, No. 2, April 1985

[47] Kara Peters, Christian Boller, Fu-Kuo Chang, Yozo Fujino Fiber-Optic Sensor Principles Encyclopedia of Structural Health Monitoring, 1 (2009)

[48] M. Kyoto, Y. Ohoga, S. Ishikawa, Y. Ishiguro Characterization of fluorine'doped silica glasses JOURNAL OF MATERIALS SCIENCE 28 (1993) 2738-2744

[49] Haynes, William M., ed. (2011). CRC Handbook of Chemistry and Physics (92nd ed.). Boca Raton, FL: CRC Press. ISBN 1439855110.

[50] R Le Parc1, C Levelut1, J Pelous, V Martinez and B Champagnon Influence of fictive temperature and composition of silica glass on anomalous elastic behavior 2008 J. Phys.: Condens. Matter 21 079802